JCI The Journal of Clinical Investigation

Type 2 deiodinase–dependent surge in thyroid hormone controls muscle stem cell quiescence and self-renewal

Maria Angela De Stefano, Raffaele Ambrosio, Cristina Luongo, Tommaso Porcelli, Daniela Di Girolamo, Caterina Miro, Monica Dentice, Caterina Missero, Domenico Salvatore

J Clin Invest. 2026. https://doi.org/10.1172/JCI194925.

Research In-Press Preview Endocrinology Metabolism

Graphical abstract

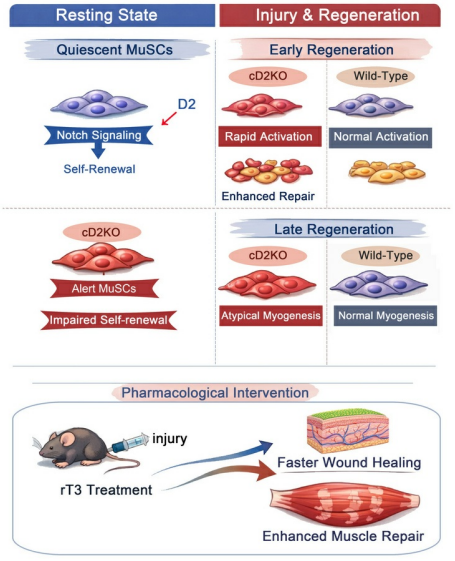

Type 2 deiodinase–dependent surge in thyroid hormone controls muscle stem cell quiescence and self-renewal.

Maria Angela De Stefano[1], Raffaele Ambrosio[1], Cristina Luongo[2], Tommaso Porcelli[1], Daniela Di Girolamo[3,4], Caterina Miro[2], Monica Dentice[2], Caterina Missero[3,4] and Domenico Salvatore[1, 4].

[1]Department of Public Health, University of Naples "Federico II", Naples, Italy;

[2]Department of Clinical Medicine and Surgery, University of Naples "Federico II", Naples, Italy;

[3]Department of Biology, University of Naples "Federico II", Naples, Italy;

[4]CEINGE Biotecnologie Avanzate Franco Salvatore, Naples, Italy.

Correspondence should be addressed to D.S.

Dipartimento di Sanità Pubblica

Università degli Studi di Napoli "Federico II"

Via S. Pansini 5, 80131

Napoli - ITALY Tel: +39 081 7463780

email: domsalva@unina.it

Running Title: Thyroid hormone in quiescent stem cells.

The authors have declared no conflict of interest.

Abbreviations: muscle stem cells (MuSCs); cross sectional area (CSA); thyroid hormone (TH); type 2 deiodinase (D2); type 3 deiodinase (D3).

ABSTRACT

Stem cells are critical for the homeostasis of adult tissues. Thyroid hormone (TH), whose intracellular concentration is increased by type 2 deiodinase (D2), is involved in many functions, but its role in quiescence is unknown. Here we show that D2 marks quiescent stem cells in muscle and skin. Genetic D2-depletion in quiescent muscle stem cells triggers their transition from G_0 to a G_{Alert} –like state. This increases the proliferative potential of the stem cells, but impairs their self-renewal capacity, leading to depletion of the stem cell pool and regenerative failure over time. Mechanistically, TH sustains Notch signaling, and active Notch overexpression partially rescues D2-depletion. Transient pharmacological inhibition of D2 accelerates muscle regeneration and skin wound healing by promoting stem cell expansion. In conclusion, we show that D2 is a critical metabolic enzyme in maintaining stem cell quiescence and in regulating self-renewal.

INTRODUCTION

Stem cells sustain tissue homeostasis by generating tissue progeny while self-renewing through cell division (1-3). This process is necessary to ensure continuous tissue maintenance in various organs, and most of the stem cell properties, namely quiescence, self-renewal and differentiation, are controlled by the stem cell microenvironment (4-8). Adult resident skeletal muscle stem cells (MuSCs), also known as satellite cells, are normally mitotically quiescent with an extremely low cell turnover, but can enter the cell cycle when activated in response to various stresses (9). As an example, upon injury quiescent MuSCs (qMuSCs) are rapidly activated and generate transient amplifying cells that undergo multiple cell divisions before differentiating to repair the injured muscle (8).

A major advance in this regard was the identification of an intermediate state between the G_0 (quiescent state) and G_1 phases of the cell cycle, termed "G_{Alert}", in which MuSCs are rapidly primed to enter the cell cycle in response to injury (10, 11). The G_{Alert} phase is induced by the circulating hepatocyte growth factor activator (HGFA), which is released into the bloodstream from the injured muscle to systemically prime qMuSCs in distant muscles, thereby accelerating tissue repair in the event of a second injury(12).

We previously demonstrated that the intracellular TH concentrations in MuSCs vary dramatically during their transition to the active state, as well as in their subsequent differentiation. These variations depend on the action of the deiodinase enzymes named D2 and D3 (13-17). Specifically, D2 converts the pro-hormone thyroxine (T4) into the active hormone triiodothyronine (T3), whereas D3 converts T3 into diiodothyronine (T2) and T4 to reverse T3 (rT3) respectively, both of which are considered nearly inactive TH metabolites. We have previously shown that a surge in D3 and the consequent reduction in intracellular TH concentration is necessary for the activation and expansion of MuSCs (18). In the later phase of the myogenic process, following MuSCs activation, D3 declines while D2 surges, thereby

increasing intracellular T3 which is required for proper muscle cell differentiation (18, 19). Whether and how the regulation of TH action by deiodinases takes place in the context of qMuSCs is completely unknown.

Notably, muscle is not the only tissue in which local TH concentrations are finely tuned during adult life. TH is also an important regulator of the skin cell development and homeostasis (20-22). Clinical evidence (23, 24) and studies conducted in hypothyroid rodents (25) suggest indeed that TH is profoundly involved in epidermal proliferation and differentiation, hair growth, and skin wound healing.

The aim of this study was to investigate if and how TH signalling is involved in the control of stem cell quiescence. We identified D2 as a marker of quiescent stem cells in both muscle and skin. Using inducible genetic models to specifically ablate the D2 gene (*Dio2*) in stem cells, we demonstrated that TH-produced D2 maintains the quiescent state in both muscle and skin stem cells and regulates the stem cell self-renewal. We provide evidence that in the muscle the maintenance of quiescent state is partially achieved through sustained Notch signalling, which is a master regulator in maintaining undifferentiated state in quiescence and homeostasis through its action in the self-renewal (26-29). In addition, we have shown that D2-depletion induces a transition of qMuSCs from a G_0 to a G_{Alert} –like state, which markedly accelerates their activation and the tissue repair upon injury.

In conclusion, here we show a pathway by which TH signalling regulates quiescence in two relevant stem cell compartments. This process requires a cell-autonomous mechanism capable of increasing intracellular TH levels and adapting them to the specific metabolic needs of quiescent stem cells.

RESULTS

D2 marks qMuSCs and preserves their quiescence.

We analysed D2 expression within the different subset of MuSCs (Tg:Pax7-nGFP cells) fractionated into distinct subpopulations based on GFP intensity. D2 expression was highest in Pax7-nGFP^{Hi} cells, the most quiescent Pax7 subset (Supplemental Figure 1A and (18)). Correspondingly, in freshly isolated MuSCs, D2 expression was elevated in quiescent cells and was dramatically reduced upon cell proliferation (Supplemental Figure 1B). Based on these findings, we speculated that D2 might mark qMuSCs. To address this hypothesis, we analysed D2 expression by immunofluorescence in resting tibialis anterior (TA) muscle. Using our previously generated 3xFLAG-D2 knock-in mouse (30), we found that D2 colocalized with the MuSCs marker Pax7 in resting TA muscle (31) (Figure 1A). Interestingly, in isolated myofibers, D2 was highly expressed and co-localized with Pax7^{+} cells immediately after fiber isolation (T0), and its expression declined after 48 hours upon MuSC activation (T48, Figure 1B). Accordingly, D2 was not detectable in proliferating cells identified by EdU incorporation, and its expression was inversely correlated with the deiodinase D3, a metabolic marker of proliferative MuSCs (18) (Figure 1C). Consistent with the role of D2 in enhancing the intracellular TH signalling machinery, we observed that other components of the TH signal machinery, namely D3 (*Dio3*), the *Thra1, Thra2* and *Thrb* receptors, the *Mct8*, *Mct10* and *Oatp1c1* transporters, were expressed in qMuSCs and decreased or increased accordingly as the cells transitioned from a quiescent to an activated state, as evidenced by the expression of the corresponding cell markers (see e.g. *Pax7, MyH2, Heyl*, Supplemental Figure 1C-L).

Given the high expression of D2 in qMuSCs, we hypothesized that D2 may have a role in preserving the quiescent state. To test this, we analysed the effects of D2 depletion in Tg:Pax7$^{CreERT2/+}$;

$D2^{fl/fl}$ mice (cD2KO), in which treatment with tamoxifen (TAM) induces D2 depletion in approximately 80% of qMuSCs (Supplemental Figure 2A). Genetic D2 depletion *in vivo* before culturing myofibers resulted in a higher percentage of $Pax7^+/MyoD^+$ (activated MuSCs) and a lower percentage of $Pax7^+/MyoD^-$ (qMuSCs) and $Pax7^-/MyoD^+$ cells (differentiating MuSCs) at different time points (Figure 1D, E). A similar effect was also observed when we blocked D2 in cultured myofibers with rT3 (a specific D2 inhibitor) for 72 hours (Supplemental Figure 2B). After rT3 treatment, we observed a decreased percentage of qMuSCs and an increased percentage of activated MuSCs compared to controls (Supplemental Figure 2C-D).

Accordingly, in myofibers treated with cytosine β-D-arabinofuranoside (AraC, a chemotherapeutic drug that kills cycling and spares quiescent cells), we detected fewer AraC-resistant $Pax7^+$ cells in the absence of D2 compared to wild-type (Supplemental Figure 2E-G). This result suggests that D2-depleted MuSCs are more prone to proliferate, and that TH locally produced by D2 may be involved in maintaining stem cells properties.

Therefore, we asked whether exogenously added TH could affect stem cell properties *in vitro*. Freshly isolated FACS sorted MuSCs cultured in the presence of additional TH (3 nM T3 and T4) for 5 days showed reduced cell proliferation (Supplemental Figure 3A, B). Interestingly, cells treated with TH remained in a Pax^+/EdU^- state compared to untreated controls, suggesting that TH treatment delayed the proliferation of MuSCs *in vitro* (Supplemental Figure 3C, D).

Genetic D2-depletion accelerates the early phase of muscle regeneration through a faster activation and proliferation of MuSCs.

To evaluate the role of D2 in muscle regeneration, we analysed TA muscles from cD2KO mice collected at 7 and 21 days after cardiotoxin (CTX) injection (Figure 2A). At 7 days post-CTX, hematoxylin/eosin staining and CS analysis revealed larger fiber sizes in cD2KO compared to wt mice

(Figure 2B, C). The number of activated $Pax7^+/MyoD^+$ was increased upon D2 deletion compared to wt mice whereas the number of quiescent $Pax7^+/MyoD^-$ was reduced (Figure 2D, E), indicating that D2 depletion promoted MuSCs proliferation. This is not due to an increased number of satellite cells already present in D2KO mice at the time of injury (Supplemental Figure 4A, B). Embryonic Myosin Heavy Chain (eMyHC) - a marker of regeneration - and laminin were already expressed as early as 3 days after injury in cD2KO, whereas they were barely detectable in wt mice (Supplemental Figure 4C, D a-b, and E). At 5 days after the injury, a residual increase in the expression of eMyHC was still observed in the cD2KO, whereas it rapidly increased in the wt at this time point (Supplemental Figure 4C, D c-d and E). At 7 days, eMyHC staining was reduced in both mouse models (Supplemental Figure 4C, D e-f and E).

Later on, at 21 days post CTX, D2-depletion resulted in an increased number of fibers with a smaller diameter (Figure 2F, G). While the number of $Pax7^+/MyoD^+$ cells was still higher at this time in cD2KO mice compared to wt controls, the number of $Pax7^+/MyoD^-$ cells was lower than wt (Figure 2H-I). The faster activation of satellite cells led to an increased muscle mass in GC measured at 21 days post-injury (Supplemental Figure 5A-C). FACS analysis of GFP^+/EdU^+ cells at 21 days post-injury confirmed the increased number of proliferating satellite cells (Supplemental Figure 5D, E). Collectively, these data suggest that the absence of D2 promotes stem cells proliferation while delaying the completion of the myogenic program. This is consistent with the role of D2 in promoting cell differentiation at the late phase of myogenesis (19). Interestingly, 60 days after CTX injury, fiber diameter in cD2KO mice became larger than in wt, suggesting that the maturation delay in D2-depleted fibers can be overcome with prolonged time (Supplemental Figure 5 F-H), and this is in agreement with the larger skeletal muscle fibers that occur during hypothyroidism in humans (32).

Taken together, these data suggest that there is a more rapid activation of qMuSCs in cD2KO mice that allows a faster initiation of the regeneration. This advantage is then lost later, when the completion of the myogenic program is delayed and does not occur normally in absence of D2.

D2 is required for self-renewal of qMuSCs.

A characteristic of stem cells is their ability to self-renew and to maintain a constant number. When proliferating MuSCs are induced to differentiate, a proportion of them escape terminal differentiation, arrest their cell cycle in the G_0 phase and return to quiescence. These mononuclear cells retain the self-renewal capacity, acquire stem cell properties, and become the so-called "reserve cells". While the $MyoD^+$ cells become positive for myogenin and irreversibly enter terminal differentiation, the other $MyoD^-$ cells remain undifferentiated, resulting in the "reserve cell" population (33-36).

The reduction in the number of qMuSCs upon D2-depletion ($Pax7^+/MyoD^-$; shown in Figure 2D-E and H-I) prompted us to investigate whether D2 plays a role in the return to quiescence, i.e. to analyse whether activated MuSCs can re-enter quiescence in the absence of D2. To this end, freshly isolated MuSCs were cultured in growth medium for 3 days and induced to differentiate for 4 days after genetic removal of D2 with 4OH-TAM (Supplemental Figure 6A). We observed a reduced capacity to generate $Pax7^+/MyoD^-$ (reserve cells) in the absence of D2, which was properly rescued by adding the D2-product T3 to the medium (Supplemental Figure 6B, C). To ensure that we were properly assessing the self-renewing population, we also performed immunofluorescence for MyHC2 to mark differentiated cells and calculated the fusion index (Supplemental Figure 6D, E). Notably, the fusion index was significantly lower in D2KO cells compared to wt, and was also rescued in T3-treated cells (Supplemental Figure 6E). Collectively, these data indicate that D2KO MuSCs have impaired capacities for both self-renewal and to differentiate, both of which were rescued by the addition of T3. Consistent with this, while proliferating $Pax7^+/MyoD^+$ cells were increased, $Pax7^-/MyoD^+$ cells were slightly reduced upon D2 depletion (Supplemental Figure 6B, C). Notably, a similar reduction in reserve cells was obtained by blocking D2 in MuSCs with rT3 treatment (Supplemental Figure 6F, G).

To evaluate whether D2-depleted MuSCs could normally reconstitute the stem cell pool *in vivo*, we analysed muscle repair after five consecutive CTX injuries, at 30 days after the last CTX (Figure 3A). After multiple injuries, the number of quiescent ($Pax7^{+}/MyoD^{-}$) MuSCs was lower in cD2KO mice (Figure 3B). Furthermore, the areas of non-muscle tissue were larger in cD2KO mice compared to control (Figure 3C, D), while the diameter of the formed muscle fibers was reduced (Figure 3E). Correspondingly, we observed an increased intramuscular fibrosis, confirming the partial inability of MuSCs to regenerate in cD2KO after successive injuries (Figure 3F, G). Collectively, these data indicate a self-renewal deficiency of D2-depleted MuSCs, leading to a gradual depletion of resident stem cells and a consequent increased fibrosis after multiple muscle injuries.

To measure the effects of long-term D2 depletion in resting muscles, we quantified the number of satellite cells by FACS analysis at both 3 and 8 months after D2 depletion. Importantly, a significant reduction in the number of D2-depleted MuSCs was observed compared to wt cells (Figure 3H-I).

To further expand on the long-term consequences of D2 depletion in resting conditions, we compared Tg:$Pax7^{CreERT2/+}$; $R26^{mTmG}$; $D2^{fl/fl}$ versus Tg:$Pax7^{CreERT2/+}$; $R26^{mTmG}$; $D2^{+/+}$ 4 months after D2-depletion (Supplemental Figure 6H). Under resting conditions, we observed that the newly generated fibers receiving D2-depleted MuSCs (green) were more numerous and smaller compared to wt fibers (Supplemental Figure 6I-K).

Taken together, these results suggest that in the long-term, physiological stimuli of muscle turnover, when acted upon abnormally alerted MuSCs as in chronic D2 depletion, determine an increased number of newly generated fibers compared to wt muscles and a reduction in the stem cell pool.

D2 sustains the Notch pathway in quiescent cells.

We analysed the cellular transcriptome in qMuSCs isolated from resting muscles of cD2KO

versus wt mice. Approximately thirteen hundred genes were significantly altered by D2 depletion, of which approximately half were upregulated, and half were downregulated (Figure 4A). By functional analysis, we identified several pathways affected by D2-depletion. Interestingly, among the upregulated pathways, cell cycle stood out as significant pathways induced by D2 depletion (Figure 4B), whereas among the downregulated pathways, the Notch signalling stood out as a potential regulator of stemness (Figure 4C).

The expression of key components of the Notch pathway was significantly reduced in FACS-isolated qMuSCs from cD2KO mice, including Notch target genes (Heyl, Hes2, Rbpj) and Notch receptors (Notch1–4) (Figure 4D). Consistently, protein levels of the active Notch1 intracellular domain (N1ICD) were reduced in D2-depleted qMuSCs (Figure 4E). Thyroid hormone (TH) treatment for 24 and 60 hours induced a time-dependent increase in N1ICD levels, indicating progressive activation of Notch signaling, and was accompanied by increased expression of downstream Notch target genes (Supplemental Figure 7A–D).

To determine whether TH regulates Notch target gene expression exclusively through canonical Notch activation, cells were treated with the γ-secretase inhibitor DAPT in the presence or absence of TH. DAPT effectively suppressed N1ICD generation (Supplemental Figure 7E). Despite blockade of Notch activation, TH maintained induction of Heyl and Notch3 expression, whereas Hes1 and Hes2 expression was markedly reduced (Supplemental Figure 7F–I), indicating differential dependence of Notch-associated genes on NICD-mediated signaling.

We next assessed direct binding of TH receptor alpha (THRα) to regulatory regions of Notch2 and Notch3. ChIP analysis demonstrated robust THRα occupancy at promoter/proximal regions of both loci (Supplemental Figure 7J), with up to ~40-fold enrichment at Notch2 and ~35-fold enrichment at Notch3 (Figure 4F, G). Notably, THRα binding at these sites was reduced to background levels in rT3-treated or D2KO cells (Figure 4H and Supplemental Figure 7K–M).

Together, these results demonstrate that D2-dependent TH signaling promotes Notch pathway activity in qMuSCs through both canonical Notch activation and direct THRα-mediated transcriptional regulation of some Notch related genes, including Notch2 and Notch3.

To assess whether active Notch could functionally rescue D2 depletion *in vivo*, we generated $Pax7^{CreERT2/+}$; $D2^{fl/fl}$; $R26^{stop\text{-}N1ICD\text{-}nGFP}$ (hereafter referred to as cD2KO-N1ICD) mice in which D2 was deleted in MuSCs with simultaneous Notch overactivation (Figure 4I). We compared the ability of the MuSC population from cD2KO/N1ICD and cD2KO mice to regenerate TA muscles 21 days after CTX injury. Immunofluorescence staining revealed a significant reduction in the number of activated $Pax7^{+}/MyoD^{+}$ cells and a corresponding increase in quiescent $Pax7^{+}/MyoD^{-}$ cells in cD2KO/N1ICD mice compared to cD2KO control (Figure 4J, K). These data indicate that D2 is required for full -but not absolute- activity of the Notch pathway in qMuSCs, and that forced Notch activity can rescue some of the effects of D2 depletion.

Acute D2 depletion in resting muscle turns qMuSCs into a "G_{Alert} -like" state.

As mentioned, "cell cycle" was among the upregulated pathways induced by D2 depletion in MuSC isolated from resting muscles (Figure 4B). Therefore, we compared by FACS analysis the percentage of EdU^{+} MuSCs in D2-depleted *versus* wt muscles in resting, injury and alerted conditions (Figure 5A). We observed that the percentage of EdU^{+} in D2-depleted MuSCs, although did not reach that of "injured" conditions, approached that of "alerted" MuSCs in wt muscles (Figure 5B, C).

Quiescent MuSCs transition between a dormant G_0 state and a primed, non-dividing G_{Alert} state induced by systemic injury (10). To determine whether D2 depletion alone is sufficient to induce a G_{Alert} state in MuSCs, we analyzed established G_{Alert} markers in freshly isolated FACS-sorted MuSCs from resting muscles of cD2KO and wt mice. D2-depleted MuSCs displayed activation of mTORC1 signaling, as shown by increased phospho-mTOR (Figure 5D), phospho-S6 (Figure 5E), and phospho-S6K (Figure

5F), concomitant with reduced phospho-AMPK levels (Figure 5G). Consistent with a G_{Alert} phenotype, D2-depleted MuSCs showed increased mitochondrial DNA content (Figure 5H) and larger cell size (Figure 5I). These data indicate that D2 depletion is sufficient to induce an G_{Alert} state in qMuSCs *in vivo*.

In parallel, we also examined whether a change in D2 levels occurs in "alerted" wt qMuSCs. Interestingly, D2 expression was reduced in G_{Alert} cells compared to quiescent G_0 cells (controls) (Figure 5J), consistently with the observation that D2-depletion triggers the "alerting" process. Lastly, we compared *in silico* the genes differentially expressed in cD2KO versus wt MuSCs with those induced in the G_{Alert} state deposited in the GSE55490 database (Figure 5K, (10)). Interestingly, of the 678 down-regulated genes in cD2KO qMuSCs, 52 overlap with the down-regulated genes in the G_{Alert} state ($p < 2.418^{e-16}$); whereas of the 611 up-regulated genes in cD2KO qMuSCs, 26 overlap with the up-regulated genes in the G_{Alert} state ($p < 0.041$) (Figure 5L). Collectively, these data indicate that D2 depletion in qMuSCs induces a state whose transcriptional signature significantly overlaps with the G_{Alert} state and support the finding that D2-depletion alone is sufficient to the transition of qMuSCs from the G_0 to the G_{Alert}–like state.

Characterization of the mdx-D2KO mice and transplantation assays to evaluate cell engrafting potential in vivo of D2-depleted cells.

Premature exhaustion of MuSCs is a major determinant of the dystrophic process (37, 38). Therefore, we asked whether D2-depletion could affect the dystrophic phenotype of *mdx* mice. To this end, we generated *mdx*/global-D2 knock-out (*mdx*-D2KO) mice and characterized the muscle phenotype by using morphological, molecular and functional analyses. At 4 weeks postnatal, which corresponds to the peak of dystrophy, fiber size was smaller and the number of fibers with central nuclei was increased in *mdx*-D2KO mice compared to *mdx* mice (Figure 6A-C). An increased number of $Pax7^+$ cells was detected in the TA muscle of *mdx*-D2KO mice compared to *mdx* mice (Figure 6D). In addition,

Myogenin and MyoD mRNA levels were higher in *mdx*-D2KO mice compared to *mdx* controls (Figure 6E).

To assess whether D2-depletion functionally improves muscle performance in dystrophic mice *in vivo*, we tested *mdx*-D2KO versus *mdx* mice with both two-limb and four-limb hanging tests (in each case represented as the holding impulse). We observed that *mdx*-D2KO mice exhibit a significantly increased ability to resist their gravitational force compared to *mdx* mice (Figure 6F, G). Finally, we measured Pax7 and neonatal MHC (neo-MHC) mRNA levels in a period from 4 to 50 weeks postnatally, and found that both markers were higher in *mdx*-D2KO mice than in *mdx*- controls (Figure 6H). Overall, these results show that global D2 deletion in the *mdx* context results in a markedly improved muscle dystrophic phenotype.

Next, to assess whether D2-depletion translates into a cell-autonomous regenerative advantage, we tested the functional capacity of D2-depleted MuSCs to engraft *in vivo* by performing a transplantation assay. We isolated MuSCs from donor Tg:Pax7$^{CreERT2/+}$; R26^{mTmG}; D2$^{fl/fl}$ *versus* Tg:Pax7$^{CreERT2/+}$; R26^{mTmG}; D2$^{+/+}$ mice and injected them into the TA of *mdx* mice (Figure 6I). The engraftment of donor-derived MuSCs into *mdx* recipients was analysed by direct epifluorescence for GFP on TA muscle harvested 21 and 40 days after transplantation (Figure 6J). The percentage of GFP-positive D2-depleted fibers was increased at both 21 and 40 days after transplantation (Figure 6K), consistent with the increased proliferative capacity of D2-depleted cells. Cross-sectional area analysis showed that- D2-depleted fibers were smaller at 21 days and larger at 40 days compared with the control, indicating that the D2-dependent maturation defect could be compensated at a later time (Figure 6L), which is consistent with what was observed in cD2KO mice after injury (Figure 2G versus Supplemental Figure 5H).

Overall, these results indicate that D2-depleted MuSCs successfully engraft, have an increased proliferative capacity and a time-dependent delay in maturation that is compensated at later time points.

D2-depletion promotes the activation of stem cells in the skin.

To assess whether D2 expression in stem cells is restricted to muscle or is a common feature in other tissues, we analyzed the localization of D2 in skin. Interestingly, D2 expression co-localized with the hair follicle stem cell marker CD34, which marks the bulge region of the hair follicle where quiescent stem cells are localized (Supplemental Figure 8A). In addition, we found that D2 expression is dynamically regulated during the hair follicle cycle. Indeed, D2 was clearly detectable in telogen, the quiescent phase of the hair follicle cycle, almost absent in anagen and catagen and never coincided with EdU labeling (Supplemental Figure 8B). Analysis of single cell RNA sequencing of full-thickness mouse skin (39) revealed that D2 is expressed predominantly in the epidermis and outer bulge region, and directly correlates with the expression of putative skin stem cell markers in these regions (i.e. CD34 and Krt15), whereas it is not expressed in activated hair germ cells. Consistent with its expression primarily in quiescent stem cells, its expression is reduced in the anagen phase of the hair follicle (Supplemental Figure 8C).

To investigate the functional role of D2 in the hair follicle stem cells we generated an inducible skin conditional D2KO (scD2KO) mouse model (Tg:$K14^{CreERT2/+}$; $D2^{fl/fl}$). Interestingly, the percentage of $CD34^{+}$/alpha 6 $integrin^{+}$ cells (i.e. hair follicle stem cells) was significantly increased 6 days after D2 depletion (Supplemental Figure 8D), suggesting that, like to what we observed in muscle, blocking D2 in hair follicle stem cells promotes their activation.

Next, we analysed the effects of specific D2 depletion in the hair follicle compartment of mice subjected to one (T1) or three (T3) consecutive rounds of hair depilation. While D2 depletion increased the number of putative stem cells ($Sox9^{+}$/EdU^{+}) in the hair follicle bulges after a single round of depilation (T1), we observed a net decrease of $Sox9^{+}$/EdU^{+} cells at T3 compared to wt mice (Supplemental Figure 8E). Correspondingly, *Sox9* and *CD34* mRNAs were initially increased at T1,

while their expression was reduced at T3 in scD2KO compared to wt controls (Supplemental Figure 8F). This suggests that while D2 depletion initially increased the activation of skin stem cells, it led to stem cell exhaustion after subsequent rounds of amplification.

To characterize the effects of D2-depletion *in vivo* during skin regeneration, we performed a wound healing assay comparing scD2KO mice to controls. A time course experiment of regenerating epidermis showed that wound closure was significantly faster in D2-depleted epidermis than in control skin (Supplemental Figure 8G). Overall, these data indicate that D2 plays an important role in hair follicle stem cells and, importantly, its depletion enhances wound repair in adult mouse skin.

Transient pharmacological D2-inhibition accelerates tissue repair in injured muscle and skin.

To overcome the limitations of the genetic D2KO model, namely its irreversibly depletion, we used rT3 to suppress D2 activity only within a defined temporal window. Firstly, we assessed whether MuSCs isolated from rT3-treated mice behaved similarly to those from D2KO mice under resting conditions. We found that the active intracellular domain of Notch (N1ICD), was reduced in MuSCs isolated from rT3-treated mice compared to controls (Supplemental Figure 9A, B). Moreover, these cells exhibited a G_{Alert}-like state, as demonstrated by the $EdU^{+}/MuSC^{+}$ FACS analysis (Supplemental Figure 9C-E), both consistent with the phenotype of D2KO mice (Figure 4E and 5C).

We sought to determine whether pharmacological D2-blockade in a specific time window could enhance tissue recovery after injury in muscle and skin. We used rT3 to specifically block D2 activity only at the early phase of regeneration, while allowing proper D2 action at later time points (Figure 7A, B). We treated mice with oral rT3 for 10 days (-7/+3 relative to CTX injury) and sacrificed them at 7 and 21 days after CTX injury (Figure 7A). Analysis at 7 days post-CTX revealed larger fibers in the muscles of rT3-treated mice compared to untreated wt controls (Figure 7C, D), similar to what observed in the cD2KO mice. Also similar to cD2KO mice (as shown in Supplemental Figure 4C-E), eMyHC expression

was reduced in muscles from rT3-treated mice 7 days after CTX injury compared to untreated wt controls (Figure 7E). However, differently from cD2KO mice, the analysis at 21 days post-CTX showed larger fibers in rT3-treated mice compared to untreated wt controls (Figure 7F, G), indicating that the maturation delay caused by to the absence of D2 did not occur upon transient rT3 treatment. This phenotype is consistent with an enhancement of stem cell activation by the absence of D2 during the early stage of MuSCs activation, and with a functioning D2 during the later stage of maturation that prevents the delay in fiber maturation observed in the cD2KO mice. Importantly, these data suggest that a transient pharmacological blockade of D2 in injured muscle increases MuSCs activation by prompting qMuSCs in a G_{Alert}-like state, thus accelerating muscle regeneration without negatively affecting the differentiation phase.

In a similar setting, we tested whether pharmacological D2 inhibition positively affects skin wound healing. Concordantly, we found that rT3-treated mice, both before the wound or contemporarily to it, repaired wounds faster than control mice (Figure 7H-J, Supplemental Figure 9F, G).

In conclusion, we have shown that drug-induced D2-blockade within a specific time frame facilitates regeneration in different tissues and could be therapeutically exploited *in vivo*.

DISCUSSION

Cellular quiescence is a property of several adult vertebrate stem cells. How this state is regulated and maintained is a central question in stem cell biology. Here, we report that the TH-producing enzyme D2 is a key metabolic player that acts as a regulator of MuSCs quiescence. The D2-mediated action represents a functional link between the circulating TH concentrations and a cell-autonomous mechanism that allows to customize/increase intracellular TH to preserve quiescence and stem cell function.

The temporal expression pattern of D2 in MuSCs is peculiar. Indeed, *Dio2* mRNA is highly expressed in quiescence, drastically reduced upon activation and turned on again at a later stage of myogenesis to allow full differentiation (Supplemental Figure 1B). The described pattern of D2 expression is consistent with what was previously reported in mRNA datasets from quiescent and activated MuSCs (GSE47177 (40) and Supplemental Figure 1M). Our data suggest that D2 is re-expressed also in a small subset of activated MuSCs, and that the D2 re-expression is relevant to their return to quiescence (Supplemental Figure 6A-C). In the absence of D2, proliferating myoblasts fail to renew quiescent cells, ultimately leading to depletion of the stem cell pool (Figure 3H-I and Supplemental 6A-C).

The role of D2 in quiescence was previously unknown. Given the differentiating and anti-proliferative effects of TH in multiple contexts (19, 41), we propose that elevated intracellular TH in muscle and skin stem cells helps maintain quiescence by buffering activating cues from the niche. Upon niche perturbation, rapid D2 downregulation facilitates exit from quiescence. The signals that regulate D2 expression in quiescent cells are currently unknown and represent the aim of future studies. The identification of D2 as specifically expressed in quiescent stem cells adds TH signaling to the list of key players in the mechanisms controlling quiescence. Importantly, this study highlights the importance of

the D2-produced T3 at the cellular level in the stem cell compartment. The data from cD2KO mice indicate that the normal circulating T3 concentration in the bloodstream is not sufficient and that an additional amount of D2-produced T3 is required to preserve quiescence.

What are the molecular mechanisms by which D2 controls quiescence? RNA-seq analysis from quiescent MuSCs revealed that multiple pathways/signals are altered upon D2 genetic depletion, including Notch (Figure 4B, C). The Notch pathway is a key regulator of many types of adult stem cells in a variety of tissues (29). Quiescent MuSCs are characterized by elevated Notch activity, which is required for the maintenance of undifferentiated state (42),(43).

Here, we shown that the THRα directly binds to the Notch2 and Notch3 gene loci and promotes their expression (Figure 4F, G and Supplemental Figure 7J). Importantly, D2 depletion—whether induced pharmacologically or genetically—results in a marked reduction in THRα occupancy at the Notch2 and Notch3 regulatory regions (Figure 4H and Supplemental Figure 7K-M). These findings demonstrate that local D2 activity is required to sustain THR binding at these loci and directly influences THR binding at DNA binding sites. The functional association between Notch and D2 was initially supposed also by the expression profile of Pax7-^{nGFP} sorted cells, where both D2 and Notch expression reached their highest levels in the GFP^{high} MuSC subpopulation (Supplemental Figure 1A and (18)). Using different combinations of genetically modified mice with altered D2 and Notch levels, we found that D2 is epistatically located upstream of Notch in qMuSCs. Notch overexpression could partially rescue the phenotype observed upon D2 depletion *in vivo* (Figure 4I- K). However, given the pleiotropic effects of TH, it is likely that other genes/pathways regulated by TH and not compensated by Notch may influence the MuSCs behavior. Of note, differences in Notch signaling could also reflect intrinsic heterogeneity among MuSC subpopulations (e.g., MyoD^{+} versus MyoD^{-} cells), rather than exclusively direct transcriptional regulation of Notch genes by THR within an otherwise equivalent cell population.

Reserve experiments also indicated that D2 is required to return proliferating progenitor myoblasts to quiescence (Figure 3I and Supplemental Figure 6A-E). *In vivo*, D2 depletion resulted in a functional deficiency to restore the stem cell reservoir in the event of multiple challenges, as observed in muscle (Figure 3A, B) and skin (Supplemental Figure 8E-F). The role of Notch signalling in MuSCs self-renewal is consistent with the reduced self-renewal capacity observed in cD2KO cells. In this scenario, the impairment in self-renewal in D2KO MuSCs could be consequent to the down-regulation of Notch. Accordingly, the decline in $Pax7^{+}$ $MyoD^{-}$ cells in cD2KO mice was rescued by N1ICD overactivation. Given the distinct roles of Notch and TH, the phenotype resulting from D2 depletion only partially overlaps with that of Notch impairment *in vivo* (43). Moreover, stem cell number is tightly tuned to an optimal physiological set point and attempts to artificially enhance it are likely to have long-term detrimental effects.

What are the consequences of D2 depletion in quiescent MuSCs? We found that specific D2-depletion in resting muscles induces the transition from G_0 to a G_{Alert}–like state, while in the regenerative setting it promotes cell proliferation. The transition from G_0 to G_{Alert} was firstly demonstrated in resting cells by the action of systemic HGFA released upon muscle injury (12). Here we found that a decrease in intracellular TH concentration by D2-depletion is sufficient to induce a G_{Alert}–like state in the absence of other systemic cues. Mechanistically, we found that D2-depletion activates mTOR and S6K and causes a corresponding reduction in pAMPK (Figure 5D-G). The effects of D2-depletion and the corresponding reduction in TH concentration are consistent with the previously reported effects of TH treatment on stimulating pAMPK levels in C2C12 myoblasts (44). In this scenario, it is reasonable to hypothesize that the known ability of TH to induce rapid mobilization of intracellular Ca^{++} levels (44, 45) could act as a molecular trigger for calcium/calmodulin-dependent protein kinase kinase 2 activity and the subsequent pAMPK/mTORC signalling cascade. Interestingly, the molecular gene program triggered by D2 depletion is significantly consistent with the gene signature triggered by the "Alert" state (Figure 5K, L),

strongly supporting the notion that there is a large overlap between D2 depletion and the transition to G_{Alert}. Importantly, the mechanisms that cause entry into G_{Alert} also determine a reduction in D2 levels *in vivo*. The reduced level of D2 expression measured in alerted MuSCs (Figure 5J) provides important support for the association between G_{Alert} and D2 action. The molecular mechanisms for this are currently unknown, but it is reasonable to hypothesize an inhibition of D2 expression by circulating growth factors (e.g. HGFA) that normally act as alarmins in the plasma.

The phenotype observed upon D2-deletion is different from what observed upon Notch deletion. Notably, while in Notch-deleted mice (*Rbpj*-deleted) quiescent MuSCs exit from the undifferentiated state to directly differentiate and fuse(43) , in the D2-depleted model cells do not exit G_0 to differentiate, but to transit in a G_{Alert}-like state. As such, the D2-depleted phenotype substantially differs from the *Rbpj*-depleted one. Probably, while in absence of Notch, a functional D2 and normal TH levels allow cell fusion, the absence of D2-TH in the D2-depleted phenotype reduces the Notch signaling and prompt cells to transit in a G_{Alert}-like state. We believe the G_{Alert}-like state induced by D2-loss represents indeed a specific cell cycle phenotype that is not associated/dependent from the attenuation of Notch signaling. Therefore, the finding that both Notch-signaling and G_{Alert}-state are regulated by D2-TH does not imply a direct link between the two, but rather suggests that both are part of the pleiotropic effects actioned by TH. However, why D2-depleted resting MuSCs exit quiescence and remain in a G_{Alert} –like state, but without differentiating as observed upon Notch signaling-depletion? We believe that the endurance of the G_{Alert}-like state in D2-depleted MuSCs may depend on the differentiation defects/delay consequent to insufficient D2-derived TH levels(19). In support to this concept, crucial muscle differentiation transcription factors and differentiation markers - such as all members of the MHC multigene family- respond to TH (46-49).

The enhanced proliferative capacity of D2-depleted cells was confirmed by engraftment experiments, which demonstrated superior engraftment compared with controls. Accordingly, the

delayed dystrophic phenotype observed in mdx-D2KO mice is likely attributable to enhanced MuSC expansion, leading to increased myoblast production. The improved functional outcome at the peak of dystrophy is consistent with prior evidence showing that hyperthyroidism exacerbates dystrophic pathology in mdx mice (50), whereas thyroid antagonism delays disease onset and reduces muscle damage in dystrophic animal models (51, 52).

In conclusion, the TH-dependent regulatory mechanism described here provides a strategy to manipulate stem cell behavior using a circulating hormonal signal. While irreversible D2 deletion causes sustained MuSC proliferation with impaired differentiation(19), we show that transient pharmacological D2 inhibition during early regeneration induces MuSC expansion without compromising subsequent differentiation (Figure 7 and Supplemental Figure 6G), resulting in accelerated repair of injured muscle and skin.

Overall, these findings identify TH signaling as a metabolic hub governing stem cell quiescence and suggest that D2 antagonists may represent a therapeutic approach when tissue damage is anticipated, with potential applications in stem cell–based regenerative strategies.

METHODS

Sex as a biological variable

Our study examined male and female animals, and similar findings are reported for both sexes. Sex was not considered as a biological variable.

Animals

Tg:Pax7^{nGFP}, Tg:Pax7^{CreERT2} and R26^{mTmG} mice were kindly provided by Shahragim Tajbakhsh (Department of Developmental & Stem Cell Biology, Stem Cells & Development Unit, Institut Pasteur, Université Paris Cité, Paris, France) (43), Dio2$^{fl/fl}$ (53), D2-3xFLAG (30), *mdx* obtained from The Jackson Laboratory (Stock No: 001801) (54), global-D2KO (55) mice were used in this study. Gt (ROSA)26Sor$^{tm1(Notch1)Dam}$/J and C57BL/6 were obtained from The Jackson Laboratory (Stock No: 008159 and 000664 respectively). The Tg:K14-Cre^{ERT2} mouse was previously described (56). Pax7^{nGFP} and Pax7^{CreERT2} were crossed to generate Pax7^{nGFP}; Pax7^{CreERT2} mice. Pax7^{nGFP}; Pax7^{CreERT2} were further crossed with Dio2$^{fl/fl}$ mice to generate Pax7^{nGFP}; Pax7^{CreERT2}; Dio2$^{fl/fl}$ mice (hereafter referred to as cD2KO). Pax7^{CreERT2}; Dio2$^{fl/fl}$ and R26 $^{stop\text{-}N1ICD\text{-}nGFP}$ were crossed to generate Pax7^{CreERT2}; Dio2$^{fl/fl}$; R26 $^{stop\text{-}N1ICD\text{-}nGFP}$ (hereafter referred to as cD2KO-N1ICD). Pax7^{nGFP}; Pax7^{CreERT2}; Dio2$^{fl/fl}$ and R26^{mTmG} were crossed to generate Pax7^{nGFP}; Pax7^{CreERT2}; Dio2$^{fl/fl}$; R26^{mTmG} mice. K14-Cre^{ERT2} and Dio2$^{fl/fl}$ were crossed to generate K14-Cre^{ERT2}; Dio2$^{fl/fl}$ mice (hereafter referred to as skin conditional D2KO, scD2KO).

All the mice used in this study were males and females between 12-16 weeks of age (unless indicated in figures), while the mdx mice used were between 12- 50 weeks of age as indicated. Our study examined male and female animals, and similar findings are reported for both sexes.

For comparative studies, age and sex were matched in each setting. Animals were genotyped by PCR using tail DNA.

Animal study approval

Mice were housed in a pathogen-free facility at CEINGE Biotecnologie Avanzate, Naples, Italy. Experiments were performed according to the guidelines of the *Ministero della Salute* and approved by the Institutional Animal Care and Use Committee (IACUC: 167/2015-PR and 354/2019-PR). Housing conditions: temperature ~72F (~22°C), 40-60% humidity, 14/10 light/dark daily cycle.

Cell cultures and reagents

C2C12 myoblast cells were obtained from ATCC (CRL-1772) and cultured in Dulbecco's modified Eagle's medium (DMEM) (Microgem, AL007-500ML) supplemented with 20% Fetal Bovine Serum (FBS) (Microgem, RM10432-500ML), 2mM glutamine (Gibco, #25030024), 50 IU penicillin and 50µg/ml streptomycin (Gibco, #15070063) at 37°C 5% CO_2. Primary muscle stem cells (pp6) were isolated from wt and D2KO mouse model (Qu Z, Balkir L, J Cell Biol. 1998) and cultured in DMEM supplemented with 10% FBS, 10% HS, 1ng/ml bFGF (gibco #13256-029 5 ng/ml IGF -1, 2mM glutamine 50 IU penicillin and 50µg/ml streptomycin at 37°C 5% CO_2. To induce differentiation, cells at 70% confluence were switched from growth medium (20% FBS for C2C12 cells or 10% FBS and 10% HS for pp6 cells) to DMEM supplemented with 2% HS (Gibco, #16050122), 10 µg/mL insulin (Sigma-Aldrich, I2643), and 5 µg/mL transferrin (Sigma-Aldrich, T8158).

Isolation and culture of single myofibers

Single myofibers were isolated from the Extensor Digitorum Longus (EDL) muscle and incubated with 0.1% collagenase type I (Sigma Aldrich, #C9891) in DMEM at 37°C for 60-70 minutes. The muscle was then transferred to a 60-mm Petri dish containing DMEM, and individual myofibers were mechanically dissociated, under a dissecting microscope using a heat-polished glass Pasteur pipette treated with HS.

Single fibers were transferred to fetal bovine serum (FBS)-coated tissue culture dishes in DMEM/ F12 (50%) supplemented with 20% FBS, 1% penicillin-streptomycin (Gibco). Fibers were fixed in 4% paraformaldehyde (PFA) (Merck, #1.04005.1000) for 10 minutes immediately or at different time points after plating and stained with specific antibodies. 60-100 myofibers from 4 mice were collected and quantified.

For the experiments with the chemotherapeutic agent AraC (Cytosine ß-D-arabinofuranoside, Sigma Aldrich, C1768), myofibers were cultured in medium for 72 hours and then incubated with 100 µM AraC for 48 hours and fixed (day 5). For EdU incorporation assays, myofibers were incubated with 2.5 mg/mL EdU, collected and fixed with 4% PFA. EdU was detected using the Click-It kit (Invitrogen, C10337) according to the manufacturer's instructions. EdU incorporation data are expressed as the percentage of EdU^+ relative to the total number of cells as measured by DAPI.

Reserve Experiment

Freshly isolated MuSCs were cultured in growth medium (GM) for 3 days and then switched to low serum differentiating medium (DM) for another 4 days to induce differentiation as in (57). The cells were fixed and stained for Pax7/MyoD (to assess the population of non-differentiated cells, as reserve cells, $Pax7^+/MyoD^-$) and for MyHC2 (to assess the induced differentiation, calculation of the fusion index (%), as number of nuclei ≥2 in MyHC2/total number of nuclei × 100).

Western blotting

Muscle stem cells freshly isolated from cD2KO or control mice were lysed in lysis buffer (50 mM Tris-Cl [pH 8.0], 200 mM NaCl, 50 mM NaF, 1 mM dithiothreitol, 1 mM Na3VO4, 0.3% IGEPAL), and a protease inhibitor cocktail (Sigma Aldrich, P8340). Cells were boiled for 5 minutes and centrifuged at 3000 rpm for 10 minutes. Samples were loaded onto 10% SDS-PAGE gels followed by Western blotting.

Antibodies used are listed in Table S1. Antibody-labeled protein bands were detected using Immobilon Western Chemiluminescent HRP Substrate (Millipore, WBKLS0500). Gel images were analyzed using Image Lab version 5.2.1 software (Biorad Laboratories).

qRT-PCR

Total RNA was extracted from freshly sorted or cultured cells using a Qiagen RNeasy Micro Kit according to the manufacturer's instructions (Qiagen, #74004), and then reverse transcribed to cDNA using VILO reverse transcriptase (Invitrogen, #11756050) according to the manufacturer's instructions. Quantitative real-time RT-PCR was performed using an iQ5 Multicolor Real Time Detector System (Bio-Rad) with SYBR Green Master Mix (Bio-Rad, #1708882). The cyclofilin A gene was used as a housekeeping gene control for ΔCT calculations [ΔCT = (CT of target gene) - (CT of housekeeping genes)]. The primer sequences we used are listed in Table S2 in the supplemental material. Fold expression values were calculated using the 2-ΔΔCT method, where ΔΔCT = (ΔCT of treatment sample) - (ΔCT of control samples) (with the control value normalized to 1). Three technical replicates were performed for all qPCR experiments.

Chromatin Immunoprecipitation (ChIP)-qPCR

C2C12 cells (~$2x10^6$) or isolated MuSC (pp6, wt ± rT3 and D2KO) were cross-linked with 1% formaldehyde in culture medium for 10 min at room temperature (RT), after which the cells were scraped in RIPA buffer (1X PBS, 1% NP-40, 0.5% sodium deoxycholate, 0.1% SDS). The cell extract was sonicated, diluted for immunoprecipitation, and incubated with the indicated antibodies or control IgG (rabbit IgG, ab172730) overnight at 4°C. Samples were sequentially washed in low salt buffer (20 mM Tris-HCl pH8.0, 150 mM NaCl, 2 mM EDTA, 0.1% SDS, 1% Triton X-100), high salt buffer (20 mM Tris-HCl pH8. 0, 500 mM NaCl, 2 mM EDTA, 0.1% SDS, 1% Triton X-100), LiCl IP wash buffer (100

mM Tris-HCl pH7.5, 500 mM LiCl, 1% NP-40, 1% sodium deoxycholate), and 1X TE (10 mM Tris-HCl pH7.5, 0.1 mM EDTA). All washes were performed at 4oC for 5 minutes. Immunoprecipitates were eluted and de-crosslinked overnight at 65°C. DNA fragments were extracted and real-time qPCR was performed for quantification. As a negative control, real-time qPCR was performed using unrelated oligonucleotides, and the presence of equivalent amounts of chromatin in each sample was confirmed by PCR without prior immunoprecipitation (input). The primer sequences we used are listed in Table S2 in the supplemental material.

Immunohistochemistry studies

Dissected muscles were snap frozen in liquid nitrogen-cooled isopentane, sectioned (7 μm thick), and stained. For immunofluorescence staining, cells or sections were fixed with 4% PFA, permeabilized with 0.1% Triton X-100, blocked with 0.5% goat serum, and incubated with primary antibody overnight at 4°C. After several washes with PBS, cells were incubated with secondary antibodies for 1 hour at RT. Alexa FluorTM 594-, 647-, or 488-conjugated secondary antibodies were used to detect mouse primary antibodies. Images were captured using an Olympus IX51 microscope equipped with Cell∗F software or an LSM 980 confocal system equipped with ZEN software (Carl Zeiss). For hematoxylin and eosin (H&E) staining, sections were fixed in 4% PFA for 15 minutes, washed several times, and embedded in hematoxylin (Sigma Aldrich, GHS116) for 5 minutes and eosin (Sigma Aldrich, HT110216) for 5 minutes using a standard protocol. For oil red O staining (Sigma-Aldrich, O0625), sections were placed in 60% isopropanol followed by incubation in 0.5 g oil red and 1% destrin solution in 98% isopropanol for 75 min; washed in 60% isopropanol and then in water. Sections were counterstained with Mayer's hematoxylin for 2 minutes. For Sirius Red staining, sections were fixed with 4% PFA for 10 min and stained with Sirius Red solution (Abcam, Cat# ab150681) for 60-90 min at RT, protected from light.

After washing in acidified water, sections were fixed in 100% ethanol and dehydrated in 100% xylene. Sections were mounted using EUKITT.

Briefly, tibialis anterior (TA) muscles were dissected and snap frozen in liquid nitrogen-submerged isopentane. Muscle cross-sections were cut at 7 µm and stained with hematoxylin and eosin. Muscle sections were imaged at 20X magnification, analyzed and quantified using CellF*Olympus imaging software. Each individual fiber was tracked and the pixel count was calibrated to obtain the cross-sectional area (CSA) of the muscle. Approximately >1,000 fibers/mouse were quantified.

Transplantation

Approximately 1-3x10^4 FACS-isolated MuSCs obtained from 12-week-old TAM-treated Pax7$^{CreERT2/+}$; D2$^{fl/fl}$; R26^{mTmG} or Tg:Pax7$^{CreERT2/+}$; D2$^{+/+}$; R26^{mTmG} mice were resuspended in 20µl of 1xPBS containing 0.1% bovine serum albumin (BSA). The 8-week-old *mdx* mice recipients were anesthetized by intraperitoneal injection of a ketamine-xylazine cocktail. The donor MuSCs were then transplanted into the TA muscle of the *mdx* mice recipients to assess skeletal muscle regeneration. Transplantation was performed by slowly injecting 10 µl of the donor cell solution into the TA muscle using a 25 µl Hamilton syringe. Each host mouse received transplantation of MuSCs cD2KO into the left TA and MuSCs Ctr into the right TA. Twenty-one and 40 days after transplantation frozen TA muscle sections were processed for immunofluorescence. For transplantation at a longer time point (40 days post-xenograft), we treated mice with tacrolimus (an anti-rejection drug, at 2.5mg/Kg/day) in water starting 11 days after xenotransplantation.

Hair follicle cycle

The dorsal back of 3-month-old anesthetized D2KO and control mice was clamped with forceps(59). Mice were harvested at 6 days for anagen, 10 days for catagen, and 60 days for telogen, and dorsal skin was collected for molecular and histologic analysis(60).

Wound healing

The dorsal fur of the mice was shaved, and the skin was cleaned with 70% ethanol. The dorsal skin was pulled with forceps, and an 8 mm full-thickness skin wound was created along the midline using a sterile 8 mm circular biopsy punch by pressing through both layers of the skin. Skin wound healing was measured every 2-3 days by anesthetizing the animals and imaging the wounded area. Each wound site was digitally photographed using a Nikon FX-35A camera at the indicated time intervals, and the wound area were analyzed on the photographs using CellF*. Changes in wound area were expressed as a percentage of the initial wound area.

Cell size

The cell size of MuSCs was evaluated by FACS using forward scatter (FSC) analysis.

Mitochondrial DNA

DNA was extracted from approximately 50,000 freshly FACS-isolated MuSCs using the QIAamp DNA Micro Kit (Qiagen) according to the manufacturer's instructions. mtDNA was quantified by qPCR using primers amplifying the cytochrome B region on mtDNA relative to the β-globin region on genomic DNA (Table S2).

RNA-seq

For RNA-seq, RNA extraction was performed with RNeasy Mini Kit (QIAGEN). RNA was processed using NextSeq 500/550 output kit (Illumina) and sequenced using the HiSeq 4000 System (Illumina). Fastq files containing sequencing reads were aligned to the mouse genome assembly mm10 (NCBI Genome assembly GRCh38) using STAR (61) with default options. Genes with a mean of DESeq2-normalized counts ("baseMean") > 10 were considered to be expressed. Data were analyzed using Rosalind (https://rosalind.onramp.bio/), with a HyperScale architecture developed by OnRampBioInformatics, Inc. (San Diego, CA).

Data Availability

The RNA-sequencing raw data generated in this study by wt or cD2KO MuSC have been deposited in the National Center for Biotechnology Information (NCBI) in Gene Expression Omnibus (GEO) under accession code GSE270968. All data values are available in the Supporting data values document.

Hanging Tests

To evaluate the muscle functional properties of D2KO-*mdx* compared to *mdx* mice (4-6 weeks of age), we used the two-limb and four-limb hanging tests according to the described protocols (62). For the two-limb hanging test, the mouse was suspended over a metal wire which was placed at 37 cm above a cage with soft bedding. After the mouse gripped the wire with its forelimbs, the hanging time was recorded. For the four-limb hanging test, the grid of a large cage was used, that was located 25 cm above a cage with soft bedding. After the mouse was placed on the grid, it was turned upside down and the hanging time was recorded. The Holding Impulse (s*g) = Body mass (grams) x Hang Time (sec) was used for analysis. It reflects the tension (impulse) developed by the animal to maintain itself on the wire or grid against gravity for the longest period of time. C57BL/6 mice were used as an additional control for comparisons with *mdx* mice.

rT3 administration *in vivo*

Reverse-T3 (Sigma Aldrich #T0281) was administered to mice (C56BL6 mice) via drinking water at a final concentration of 2µg/mL (or PBS as control) for 10 consecutive days.

Quantification and Statistical analysis

Significant differences were calculated using ANOVA and Student's two-tailed t test for independent samples, with $p < 0.05$ considered as statistically significant. All statistics and graphics were performed using GraphPad Prism7 and are described in more detail in the SI Appendix, S20. In all figures, error bars represent the SEM. Data are presented as mean ± SEM; *$p < 0.05$, **$p < 0.01$, ***$p < 0.001$ using a Mann-Whitney test when comparing two conditions, and 2-way ANOVA when comparing plus conditions. The sample size for each experiment is given in the corresponding figure legend. A value of $p < 0.05$ was considered significant (*$P < 0.05$; **$P < 0.01$; ***$P < 0.001$).

AUTHOR CONTRIBUTIONS

M.A.D.S., R.A., C.L., T.P. and D.D.G. performed *in vitro* and *in vivo* experiments and prepared figures. Conceptualization, M.A.D.S. and D.S.; Formal Analysis, M.A.D.S.; R.A.; C.L.; D.D.G.; M.D. and C. Miro.; Investigation, M.A.D.S.; Observations and scientific interpretation, C. Missero; Writing, M.A.D.S. and D.S.; Supervision, D.S.

FUNDING SUPPORT

This research was funded by the grant from the European Research Council under the European Union's Horizon2020 Programme—EU FP7 contract THYRAGE (grant number 666869), by the PRIN Prot. 2022H8LXFR and by Associazione Italiana per la Ricerca sul Cancro AIRC (Grant IG 27729) to DS and to CM (Grant IG 25116).

ACKNOWLEDGEMENTS

We would like to thank the Advanced Light Microscopy Facility of CEINGE Biotecnologie Avanzate for the use of microscopy.

Declaration of Interests

The authors declare no competing interests.

REFERENCES

1. Brack AS, and Rando TA. Tissue-specific stem cells: lessons from the skeletal muscle satellite cell. *Cell stem cell.* 2012;10(5):504-14.
2. Feige P, Brun CE, Ritso M, and Rudnicki MA. Orienting Muscle Stem Cells for Regeneration in Homeostasis, Aging, and Disease. *Cell stem cell.* 2018;23(5):653-64.
3. Wang YX, and Rudnicki MA. Satellite cells, the engines of muscle repair. *Nature reviews Molecular cell biology.* 2011;13(2):127-33.
4. Fuchs E, and Blau HM. Tissue Stem Cells: Architects of Their Niches. *Cell stem cell.* 2020;27(4):532-56.
5. Rudnicki MA, Le Grand F, McKinnell I, and Kuang S. The molecular regulation of muscle stem cell function. *Cold Spring Harbor symposia on quantitative biology.* 2008;73:323-31.
6. Tumbar T, Guasch G, Greco V, Blanpain C, Lowry WE, Rendl M, et al. Defining the epithelial stem cell niche in skin. *Science.* 2004;303(5656):359-63.
7. Fuchs E, Tumbar T, and Guasch G. Socializing with the neighbors: stem cells and their niche. *Cell.* 2004;116(6):769-78.
8. Yin H, Price F, and Rudnicki MA. Satellite cells and the muscle stem cell niche. *Physiological reviews.* 2013;93(1):23-67.
9. Dumont NA, Bentzinger CF, Sincennes MC, and Rudnicki MA. Satellite Cells and Skeletal Muscle Regeneration. *Comprehensive Physiology.* 2015;5(3):1027-59.
10. Rodgers JT, King KY, Brett JO, Cromie MJ, Charville GW, Maguire KK, et al. mTORC1 controls the adaptive transition of quiescent stem cells from G0 to G(Alert). *Nature.* 2014;510(7505):393-6.
11. Brun CE, Sincennes MC, Lin AYT, Hall D, Jarassier W, Feige P, et al. GLI3 regulates muscle stem cell entry into G(Alert) and self-renewal. *Nature communications.* 2022;13(1):3961.
12. Rodgers JT, Schroeder MD, Ma C, and Rando TA. HGFA Is an Injury-Regulated Systemic Factor that Induces the Transition of Stem Cells into GAlert. *Cell reports.* 2017;19(3):479-86.
13. Bianco AC, Dumitrescu A, Gereben B, Ribeiro MO, Fonseca TL, Fernandes GW, et al. Paradigms of Dynamic Control of Thyroid Hormone Signaling. *Endocrine reviews.* 2019;40(4):1000-47.
14. Gereben B, Zavacki AM, Ribich S, Kim BW, Huang SA, Simonides WS, et al. Cellular and molecular basis of deiodinase-regulated thyroid hormone signaling. *Endocrine reviews.* 2008;29(7):898-938.
15. Ambrosio R, De Stefano MA, Di Girolamo D, and Salvatore D. Thyroid hormone signaling and deiodinase actions in muscle stem/progenitor cells. *Molecular and cellular endocrinology.* 2017;459:79-83.
16. Luongo C, Dentice M, and Salvatore D. Deiodinases and their intricate role in thyroid hormone homeostasis. *Nature reviews Endocrinology.* 2019;15(8):479-88.
17. De Stefano MA, Ambrosio R, Porcelli T, Orlandino G, Salvatore D, and Luongo C. Thyroid Hormone Action in Muscle Atrophy. *Metabolites.* 2021;11(11).
18. Dentice M, Ambrosio R, Damiano V, Sibilio A, Luongo C, Guardiola O, et al. Intracellular inactivation of thyroid hormone is a survival mechanism for muscle stem cell proliferation and lineage progression. *Cell metabolism.* 2014;20(6):1038-48.
19. Dentice M, Marsili A, Ambrosio R, Guardiola O, Sibilio A, Paik JH, et al. The FoxO3/type 2 deiodinase pathway is required for normal mouse myogenesis and muscle regeneration. *The Journal of clinical investigation.* 2010;120(11):4021-30.
20. Slominski A, and Wortsman J. Neuroendocrinology of the skin. *Endocrine reviews.* 2000;21(5):457-87.

21. Slominski A, Wortsman J, Kohn L, Ain KB, Venkataraman GM, Pisarchik A, et al. Expression of hypothalamic-pituitary-thyroid axis related genes in the human skin. *The Journal of investigative dermatology.* 2002;119(6):1449-55.
22. Paus R. Exploring the "thyroid-skin connection": concepts, questions, and clinical relevance. *The Journal of investigative dermatology.* 2010;130(1):7-10.
23. Bodo E, van Beek N, Naumann V, Ohnemus U, Brzoska T, Abels C, et al. Modulation of chemotherapy-induced human hair follicle damage by 17-beta estradiol and prednisolone: potential stimulators of normal hair regrowth by "dystrophic catagen" promotion? *The Journal of investigative dermatology.* 2009;129(2):506-9.
24. van Beek N, Bodo E, Kromminga A, Gaspar E, Meyer K, Zmijewski MA, et al. Thyroid hormones directly alter human hair follicle functions: anagen prolongation and stimulation of both hair matrix keratinocyte proliferation and hair pigmentation. *The Journal of clinical endocrinology and metabolism.* 2008;93(11):4381-8.
25. Safer JD, Fraser LM, Ray S, and Holick MF. Topical triiodothyronine stimulates epidermal proliferation, dermal thickening, and hair growth in mice and rats. *Thyroid : official journal of the American Thyroid Association.* 2001;11(8):717-24.
26. Bjornson CR, Cheung TH, Liu L, Tripathi PV, Steeper KM, and Rando TA. Notch signaling is necessary to maintain quiescence in adult muscle stem cells. *Stem cells.* 2012;30(2):232-42.
27. Zhou B, Lin W, Long Y, Yang Y, Zhang H, Wu K, et al. Notch signaling pathway: architecture, disease, and therapeutics. *Signal transduction and targeted therapy.* 2022;7(1):95.
28. Williams SE, Beronja S, Pasolli HA, and Fuchs E. Asymmetric cell divisions promote Notch-dependent epidermal differentiation. *Nature.* 2011;470(7334):353-8.
29. Gioftsidi S, Relaix F, and Mourikis P. The Notch signaling network in muscle stem cells during development, homeostasis, and disease. *Skeletal muscle.* 2022;12(1):9.
30. Castagna MG, Dentice M, Cantara S, Ambrosio R, Maino F, Porcelli T, et al. DIO2 Thr92Ala Reduces Deiodinase-2 Activity and Serum-T3 Levels in Thyroid-Deficient Patients. *The Journal of clinical endocrinology and metabolism.* 2017;102(5):1623-30.
31. Seale P, Sabourin LA, Girgis-Gabardo A, Mansouri A, Gruss P, and Rudnicki MA. Pax7 is required for the specification of myogenic satellite cells. *Cell.* 2000;102(6):777-86.
32. McKeran RO, Slavin G, Andrews TM, Ward P, and Mair WG. Muscle fibre type changes in hypothyroid myopathy. *Journal of clinical pathology.* 1975;28(8):659-63.
33. de Morree A, and Rando TA. Regulation of adult stem cell quiescence and its functions in the maintenance of tissue integrity. *Nature reviews Molecular cell biology.* 2023;24(5):334-54.
34. Yoshida N, Yoshida S, Koishi K, Masuda K, and Nabeshima Y. Cell heterogeneity upon myogenic differentiation: down-regulation of MyoD and Myf-5 generates 'reserve cells'. *Journal of cell science.* 1998;111 (Pt 6):769-79.
35. Collins CA, Olsen I, Zammit PS, Heslop L, Petrie A, Partridge TA, et al. Stem cell function, self-renewal, and behavioral heterogeneity of cells from the adult muscle satellite cell niche. *Cell.* 2005;122(2):289-301.
36. Zammit PS, Golding JP, Nagata Y, Hudon V, Partridge TA, and Beauchamp JR. Muscle satellite cells adopt divergent fates: a mechanism for self-renewal? *The Journal of cell biology.* 2004;166(3):347-57.
37. Ontell M. Muscular dystrophy and muscle regeneration. *Human pathology.* 1986;17(7):673-82.
38. Bianchi A, Mozzetta C, Pegoli G, Lucini F, Valsoni S, Rosti V, et al. Dysfunctional polycomb transcriptional repression contributes to lamin A/C-dependent muscular dystrophy. *The Journal of clinical investigation.* 2020;130(5):2408-21.
39. Joost S, Annusver K, Jacob T, Sun X, Dalessandri T, Sivan U, et al. The Molecular Anatomy of Mouse Skin during Hair Growth and Rest. *Cell stem cell.* 2020;26(3):441-57 e7.
40. Liu L, Cheung TH, Charville GW, Hurgo BM, Leavitt T, Shih J, et al. Chromatin modifications as determinants of muscle stem cell quiescence and chronological aging. *Cell reports.* 2013;4(1):189-204.

41. Garcia-Serrano L, Gomez-Ferreria MA, Contreras-Jurado C, Segrelles C, Paramio JM, and Aranda A. The thyroid hormone receptors modulate the skin response to retinoids. *PloS one.* 2011;6(8):e23825.
42. Conboy IM, and Rando TA. The regulation of Notch signaling controls satellite cell activation and cell fate determination in postnatal myogenesis. *Developmental cell.* 2002;3(3):397-409.
43. Mourikis P, Sambasivan R, Castel D, Rocheteau P, Bizzarro V, and Tajbakhsh S. A critical requirement for notch signaling in maintenance of the quiescent skeletal muscle stem cell state. *Stem cells.* 2012;30(2):243-52.
44. Yamauchi M, Kambe F, Cao X, Lu X, Kozaki Y, Oiso Y, et al. Thyroid hormone activates adenosine 5'-monophosphate-activated protein kinase via intracellular calcium mobilization and activation of calcium/calmodulin-dependent protein kinase kinase-beta. *Molecular endocrinology.* 2008;22(4):893-903.
45. Irrcher I, Walkinshaw DR, Sheehan TE, and Hood DA. Thyroid hormone (T3) rapidly activates p38 and AMPK in skeletal muscle in vivo. *Journal of applied physiology.* 2008;104(1):178-85.
46. Hughes SM, Taylor JM, Tapscott SJ, Gurley CM, Carter WJ, and Peterson CA. Selective accumulation of MyoD and myogenin mRNAs in fast and slow adult skeletal muscle is controlled by innervation and hormones. *Development.* 1993;118(4):1137-47.
47. Carnac G, Albagli-Curiel O, Vandromme M, Pinset C, Montarras D, Laudet V, et al. 3,5,3'-Triiodothyronine positively regulates both MyoD1 gene transcription and terminal differentiation in C2 myoblasts. *Molecular endocrinology.* 1992;6(8):1185-94.
48. Downes M, Griggs R, Atkins A, Olson EN, and Muscat GE. Identification of a thyroid hormone response element in the mouse myogenin gene: characterization of the thyroid hormone and retinoid X receptor heterodimeric binding site. *Cell growth & differentiation : the molecular biology journal of the American Association for Cancer Research.* 1993;4(11):901-9.
49. Salvatore D, Simonides WS, Dentice M, Zavacki AM, and Larsen PR. Thyroid hormones and skeletal muscle--new insights and potential implications. *Nature reviews Endocrinology.* 2014;10(4):206-14.
50. McIntosh LM, Pernitsky AN, and Anderson JE. The effects of altered metabolism (hypothyroidism) on muscle repair in the mdx dystrophic mouse. *Muscle & nerve.* 1994;17(4):444-53.
51. Sabeur K, King DB, and Entrikin RK. Differential effects of methimazole and dexamethasone in avian muscular dystrophy. *Life sciences.* 1993;52(13):1149-59.
52. Entrikin RK, and Larson DB. Avian muscular dystrophy: serum thyroid defect and limited improvement with methimazole and propylthiouracil. *Experimental neurology.* 1985;87(2):318-25.
53. Luongo C, Martin C, Vella K, Marsili A, Ambrosio R, Dentice M, et al. The selective loss of the type 2 iodothyronine deiodinase in mouse thyrotrophs increases basal TSH but blunts the thyrotropin response to hypothyroidism. *Endocrinology.* 2015;156(2):745-54.
54. Anderson JE, Liu L, Kardami E, and Murphy LJ. The pituitary-muscle axis in mdx dystrophic mice. *Journal of the neurological sciences.* 1994;123(1-2):80-7.
55. Christoffolete MA, Arrojo e Drigo R, Gazoni F, Tente SM, Goncalves V, Amorim BS, et al. Mice with impaired extrathyroidal thyroxine to 3,5,3'-triiodothyronine conversion maintain normal serum 3,5,3'-triiodothyronine concentrations. *Endocrinology.* 2007;148(3):954-60.
56. Miro C, Di Cicco E, Ambrosio R, Mancino G, Di Girolamo D, Cicatiello AG, et al. Thyroid hormone induces progression and invasiveness of squamous cell carcinomas by promoting a ZEB-1/E-cadherin switch. *Nature communications.* 2019;10(1):5410.
57. Stuelsatz P, Pouzoulet F, Lamarre Y, Dargelos E, Poussard S, Leibovitch S, et al. Down-regulation of MyoD by calpain 3 promotes generation of reserve cells in C2C12 myoblasts. *The Journal of biological chemistry.* 2010;285(17):12670-83.
58. Yan Z, Choi S, Liu X, Zhang M, Schageman JJ, Lee SY, et al. Highly coordinated gene regulation in mouse skeletal muscle regeneration. *The Journal of biological chemistry.* 2003;278(10):8826-36.
59. Plikus MV, Mayer JA, de la Cruz D, Baker RE, Maini PK, Maxson R, et al. Cyclic dermal BMP signalling regulates stem cell activation during hair regeneration. *Nature.* 2008;451(7176):340-4.

60. Stenn KS, and Paus R. Controls of hair follicle cycling. *Physiological reviews.* 2001;81(1):449-94.
61. Dobin A, Davis CA, Schlesinger F, Drenkow J, Zaleski C, Jha S, et al. STAR: ultrafast universal RNA-seq aligner. *Bioinformatics.* 2013;29(1):15-21.
62. Aartsma-Rus A, and van Putten M. Assessing functional performance in the mdx mouse model. *Journal of visualized experiments : JoVE.* 2014(85).

FIGURES

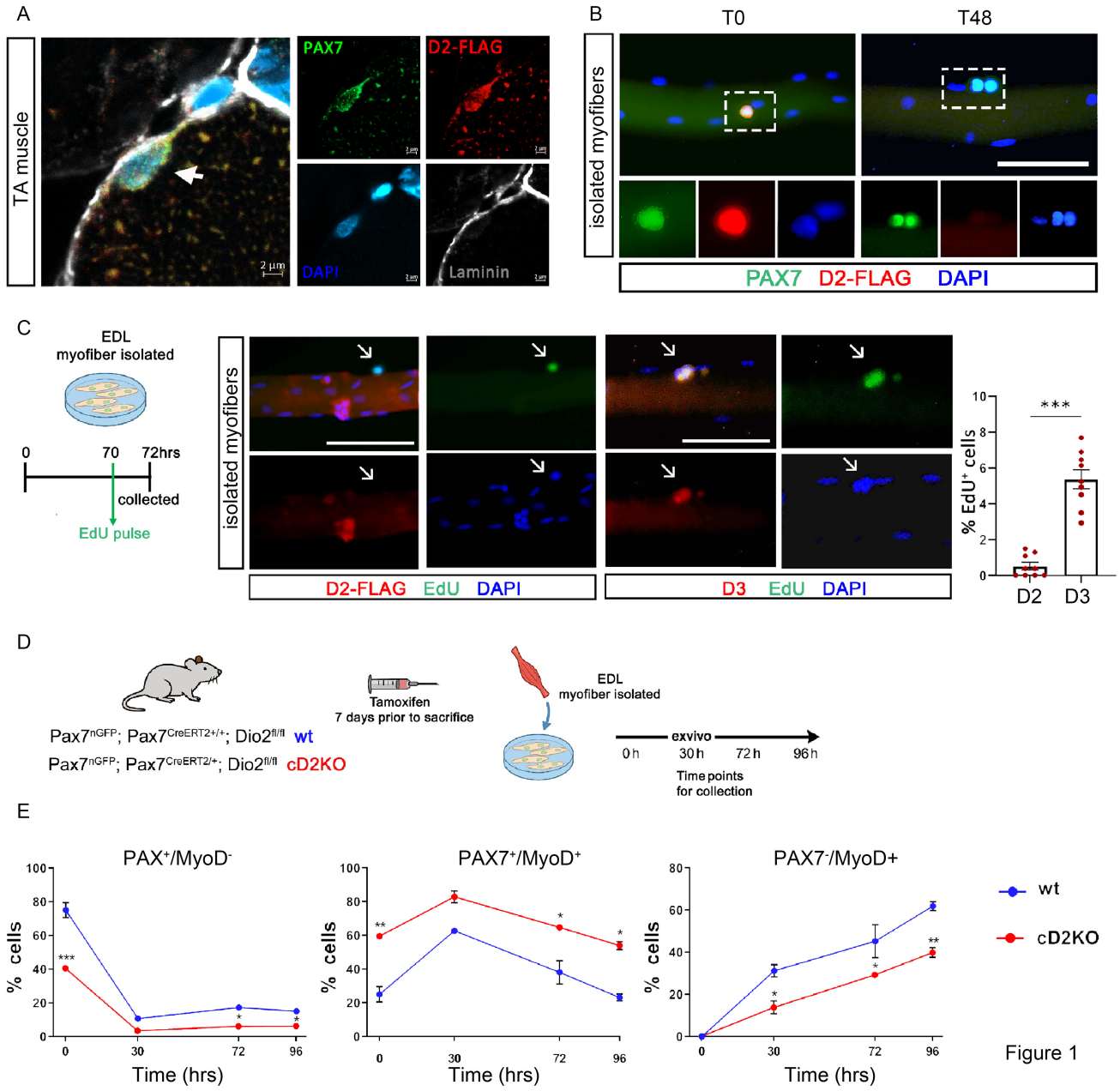

Figure 1

Figure 1. ***D2 is highly expressed in qMuSCs and its deletion favours cell activation.***

A) Representative immunofluorescence (IF) of PAX7, D2 and Laminin co-localization. Confocal images of PAX7 (green), D2-FLAG (red), Laminin (white) and DAPI (blue) expression on cryosections of tibialis anterior (TA) muscle from D2-FLAG mice (Scale bar, 2 μm).

(B) Single myofibers with associated MuSCs were immunostained for PAX7 (green) and D2-FLAG (red) (Scale bar, 50 μm, T = hours).

(C) Schematic diagram of the experimental design and representative IF staining for both D2 and D3 versus EdU in cultured fibers at 72 hours (scale bar, 50 μm). To the right, quantification of the percentage of D2+/EdU+ and D3+/EdU+ cells (n=9 mice for D2, n=9 mice for D3).

(D) Schematic diagram of the experimental design and mouse model used (D, E).

(E) Quantification of the percentage of PAX7+/MyoD-, PAX7+/MyoD+ and PAX7-/MyoD+ cells on isolated myofibers, after in vivo TAM induction, at different time points (n=5 wild type and n=4 cD2KO mice). Data are presented as mean ± SEM; *$p < 0.05$, **$p < 0.01$, ***$p < 0.001$ using a Mann-Whitney test when comparing two conditions, and 2-way ANOVA when comparing multiple conditions.

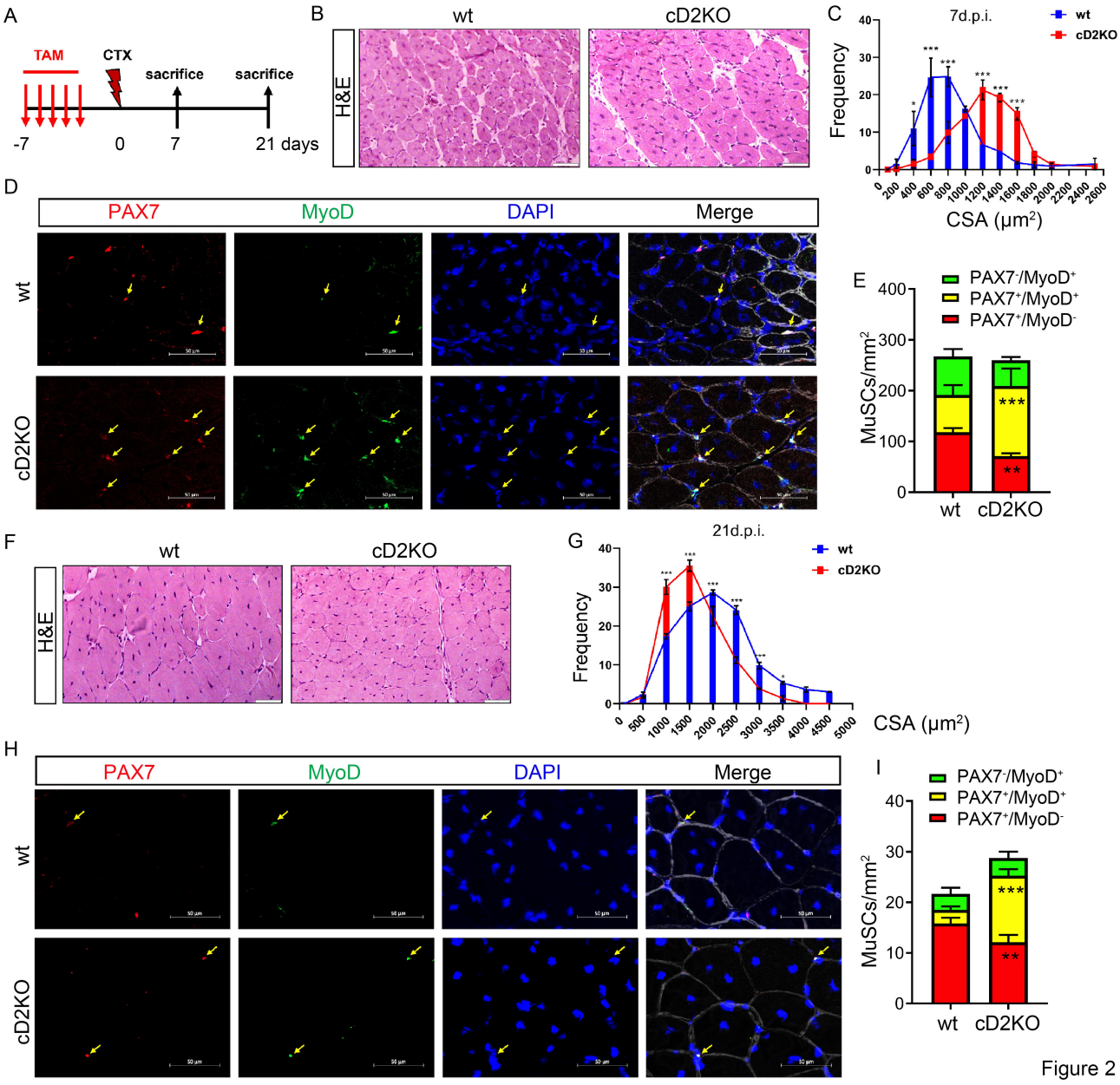

Figure 2

Figure 2. ***Absence of D2 leads to a faster proliferation of MuSCs and transiently accelerates muscle regeneration.***

(A) Schematic diagram of the experimental design, which mice were sacrificed at 7 (B-E) and 21 days (F-I). n = 9 wild type and n = 9 cD2KO mice (7days); n = 8 wild type and n = 8 cD2KO mice (21days)

(B) H&E staining of the TA sections (Scale bar, 100 μm).

(C) Quantification of the cross-sectional area of B.

(D) Representative IF staining of PAX7 (red) and MyoD (green) on TA sections. The arrows indicate $PAX7^{+}/MyoD^{+}$ cells (Scale bar, 50 μm).

(E) The number of PAX7±/MyoD± cells per mm^2 in D.

(F) H&E staining of the TA sections (Scale bar, 100 μm).

(G) Quantification of the cross-sectional area.

(H) Representative IF staining of PAX7 (red) and MyoD (green) on TA sections. The arrows indicate $PAX7^{+}/MyoD^{+}$ cells (Scale bar, 50 μm).

(I) The number of PAX7±/MyoD± cells per mm^2 in H.

Data are presented as mean ± SEM; *$p < 0.05$, **$p < 0.01$, ***$p < 0.001$ using a Mann-Whitney test when comparing two conditions, and 2-way ANOVA when comparing multiple conditions.

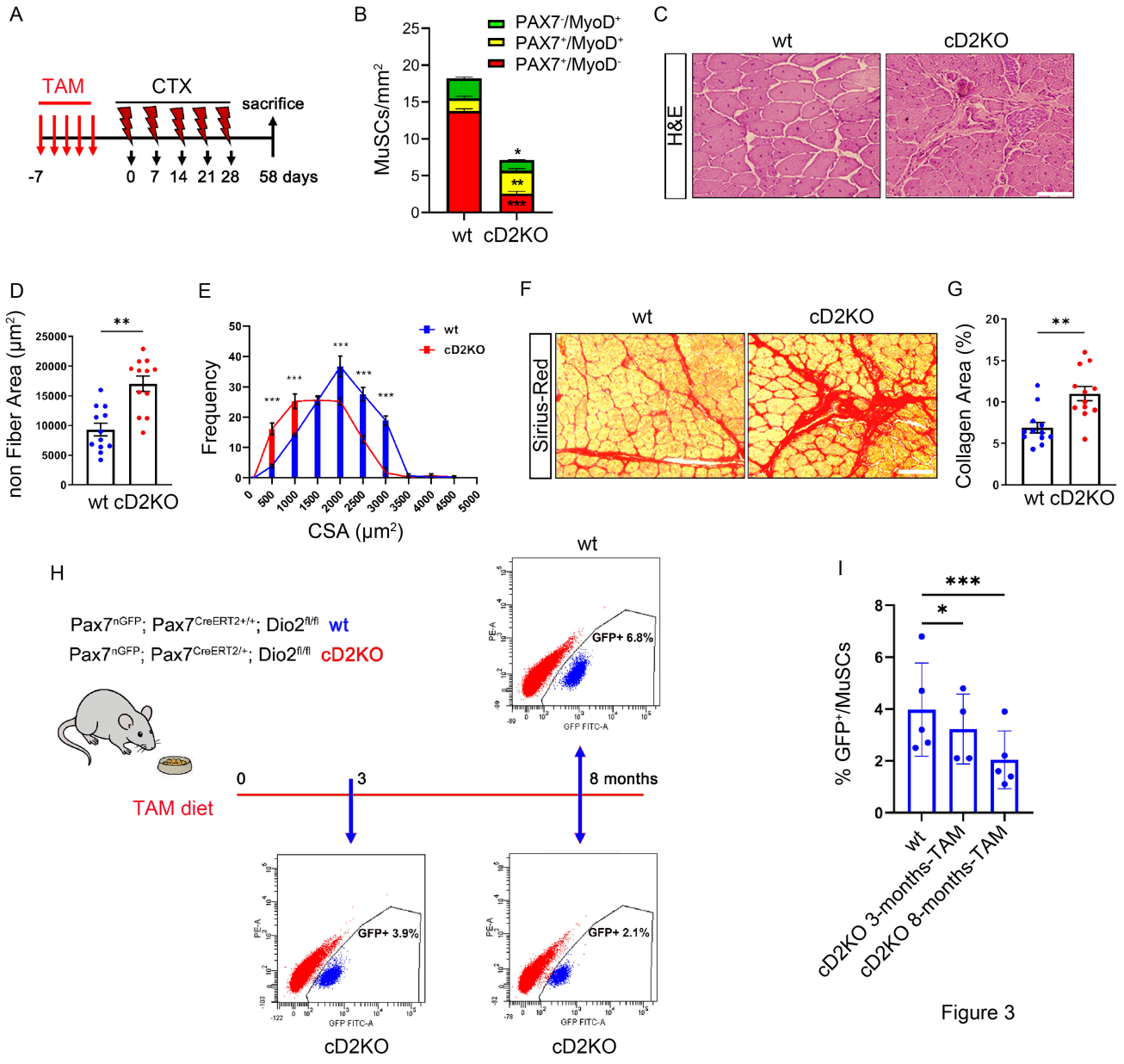

Figure 3

Figure 3. ***D2 is required for self-renewal of qMuSCs.***

(A) Schematic design of the experiment with multiple CTX injections in cD2KO and wild type mice (B-G) n =12 wild type and n=12 cD2KO mice.

(B) The number of PAX7±/MyoD± cells per mm^2.

(C) H&E of TA sections (Scale bar, 75 µm).

(D) Percentage of non-myofiber tissue.

(E) Quantification of the CSA of TA sections.

(F) Representative Sirius red staining of TA sections (Scale bar, 75 μm).

(G) Percentage of collagen area in F.

(H) Mouse model used and diagram of the experimental design. FACS analysis showing GFP+ /MuSCs cells at 3 and 8 months after D2 depletion compared to wild type mice. n=5 wild type and n= 4 (3 months) and n=8 (8 months) cD2KO mice. (I) Quantification of GFP^+/MuSCs in H.

Data are presented as mean ± SEM; *p < 0.05, **p < 0.01, ***p < 0.001 using a Mann-Whitney test when comparing two conditions, and 2-way ANOVA when comparing multiple conditions.

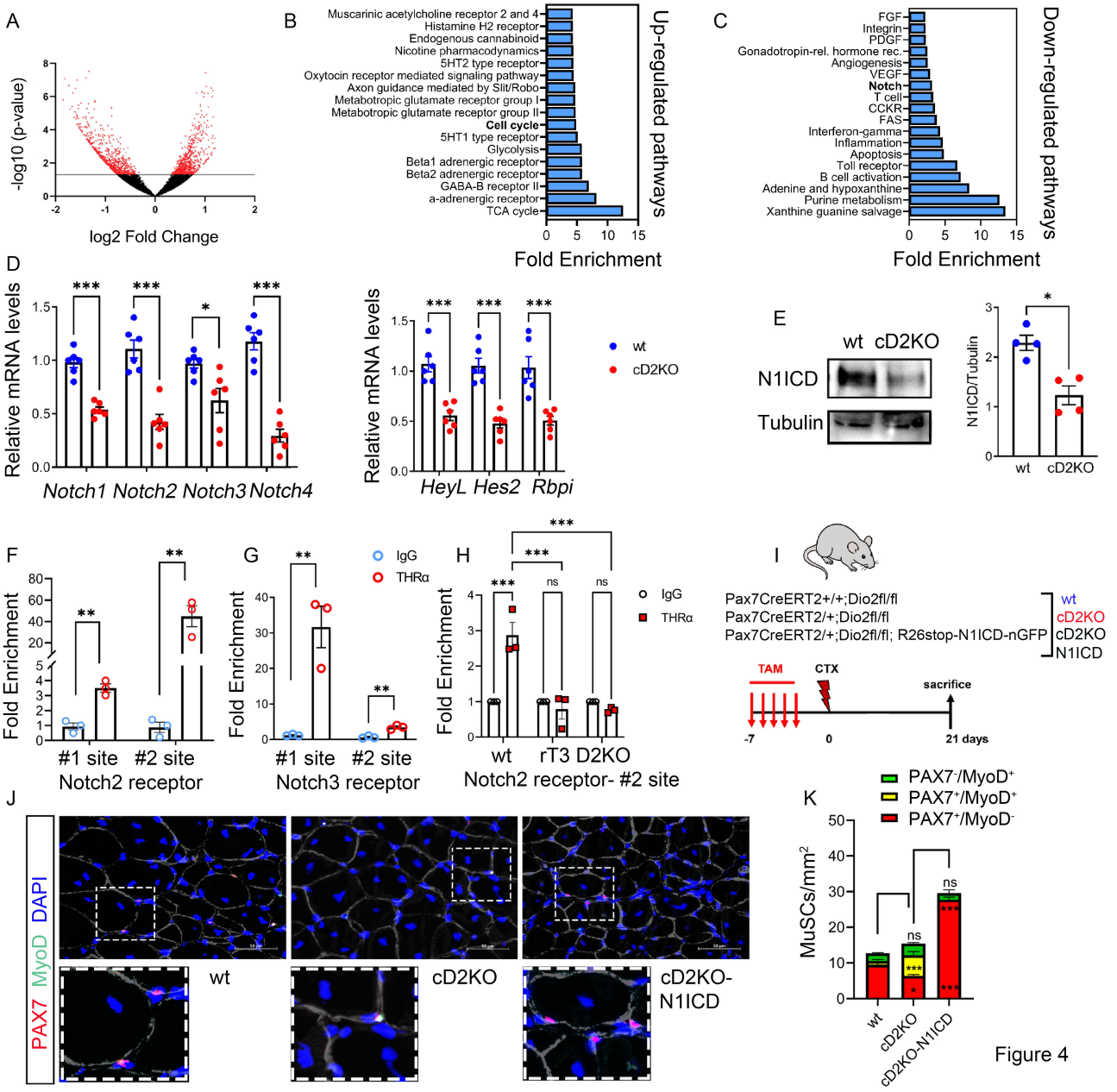

Figure 4

Figure 4. ***D2 action sustains the Notch signaling pathway.***

(A) Volcano plot showing differences in the mRNA expression of quiescent MuSCs from cD2KO and wild type mice. Negative log10 p-value (y-axis) and log2 fold change (x-axis) are plotted for transcripts detected by RNA-seq analysis. The experiments were conducted on n=3 biological replicates. Gray line indicates p-value <0.05.

(B) The top up-regulated pathways in Panther (Protein Analysis Through Evolutionary Relationships).
(C) The down-regulated pathways in Panther.
(D) mRNA levels of Notch receptors (N1-2-3-4) and Notch targets (Hey-L, Hes2 and Rbpj) in freshly isolated qMuSCs by FACS. n=6 wild type and n=6 cD2KO mice.
(E) Western blot from cD2KO and wt qMuSCs freshly isolated by FACS. The graph on the right shows the quantification of N1ICD/tubulin.
(F-G) ChIP-qPCR using THR-alpha and isotype IgG control antibodies on proximal enhancer and promoter regions of Notch2 and Notch3 genes, respectively, in C2C12 cells. Data are normalized to input chromatin (n=3 biologically independent samples).
(H) ChIP-qPCR using THR-alpha and isotype IgG control antibodies on proximal enhancer of Notch2 in freshly isolated MuSCs from wt, rT3 -treated and D2KO cells. Data are normalized to input chromatin (n=3 biologically independent samples).
(I) Mouse model used and diagram of *in vivo* rescue experiment. Two independent experiments were conducted with n=4 wild type, n=4 cD2KO and n=4 cD2KO-N1ICD mice each.
(J) Representative IF of PAX7 (red) and MyoD (green) in TA muscle from indicated mice harvested 21 days after CTX injection (scale bar, 50 μm). (K) the number of PAX7±/MyoD± cells per mm^2. Bars represent the average of at least three technical replicates. n=8 mice for each group. Data are presented as mean ± SEM; *$p < 0.05$, **$p < 0.01$, ***$p < 0.001$ using a t-student test when comparing two conditions, and 2-way ANOVA when comparing multiple conditions.

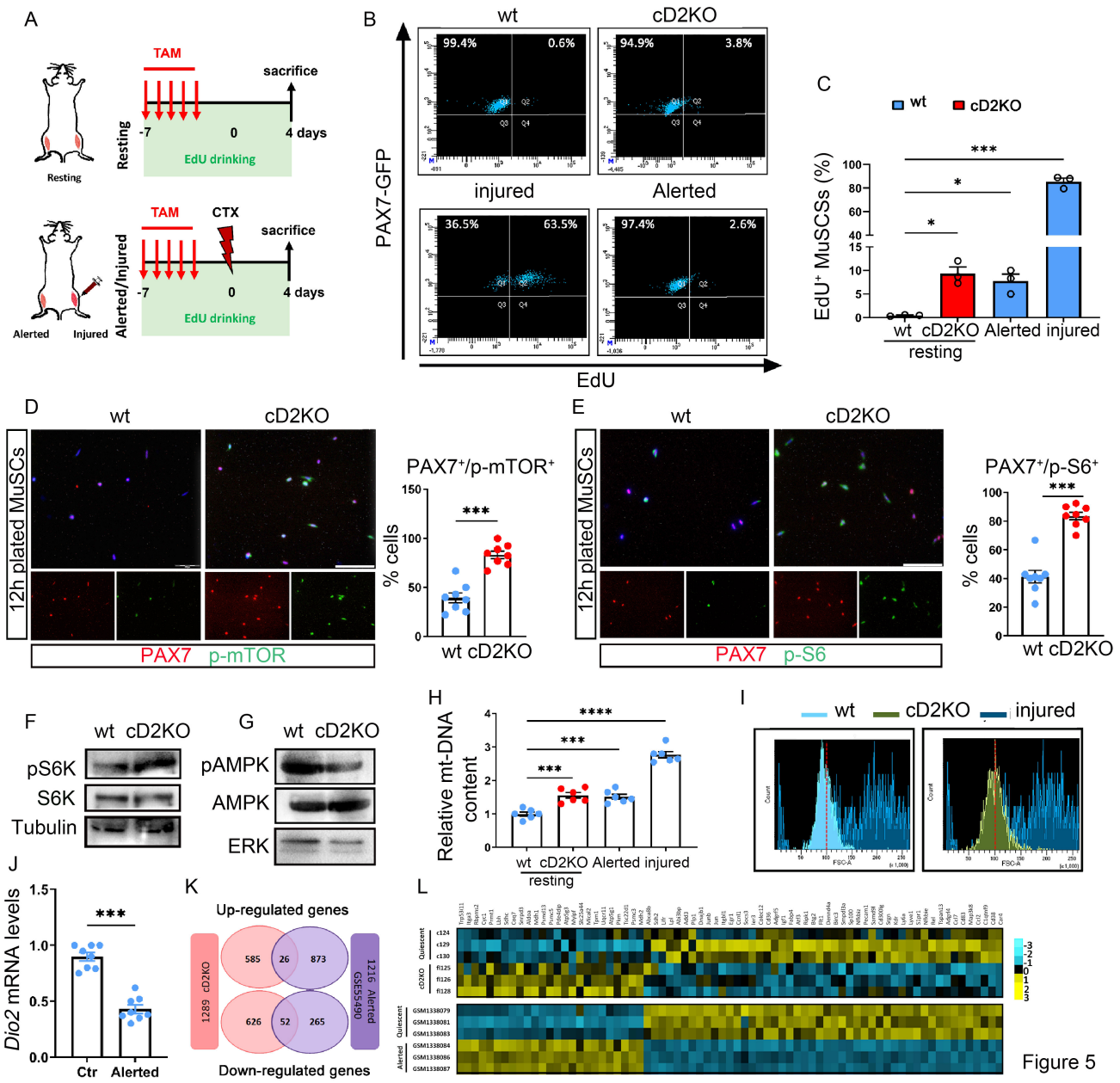

Figure 5

Figure 5. ***D2 depletion turns qMuSC in an "alert state".***

(A) Schematic representation of the experiment.

(B) Representative FACS plots for EdU/Pax7-GFP of MuSCs isolated from resting TA muscle of indicated mice (upper panels) and from alerted and injured muscles of wt mice (lower panels).

(C) Percentage of EdU+/MuSCs in B. n=4 independent experiments with n=3 wt and cD2KO mice.

(D and E) Representative IF for PAX7, p-mTOR (D) and p-S6 (E) in FACS-isolated MuSCs from resting wt and cD2KO mice (scale bar, 200 μm), and respective quantification of the percentage of PAX7±/p-mTOR± cells (D) and PAX7±/pS6± cells (E) (n= 8 wt and n=8 cD2KO mice).

(F and G) Western blot for pS6K and total S6K (F) and pAMPK and total AMPK (G). Tubulin and ERK served as a loading control.

(H) Relative content of mitochondrial DNA in FACS-isolated MuSCs from resting wt, resting cD2KO, alerted wild type and injured wt mice muscles (n=6 wt and cD2KO mice).

(I) Representative FACS histogram of forward scatter (FSC) signal of MuSCs from resting wt (light blue), resting cD2KO (green) and injured wt (blue) muscles.

(J) Dio2 mRNA levels of MuSCs from wt muscles in resting (ctr) and alerted conditions. Alerted MuSCs were harvested 2 days after CTX in contralateral tibialis anterior muscle (n=8 wt and cD2KO mice).

(K) Venn comparison analysis between cD2KO RNA-seq and G_{Alert} state array (10), common genes downregulated ($p < 2.418e-16$) and common genes upregulated ($p < 0.041$) are shown.

(L) Heatmap comparison of common genes up/down- regulated from cD2KO RNA-seq versus Ctr (quiescent) and G_{Alert} state array previously described (10).

Data are presented as mean ± SEM; *$p < 0.05$, **$p < 0.01$, ***$p < 0.001$ using a Mann-Whitney test when comparing two conditions, and 2-way ANOVA when comparing multiple conditions.

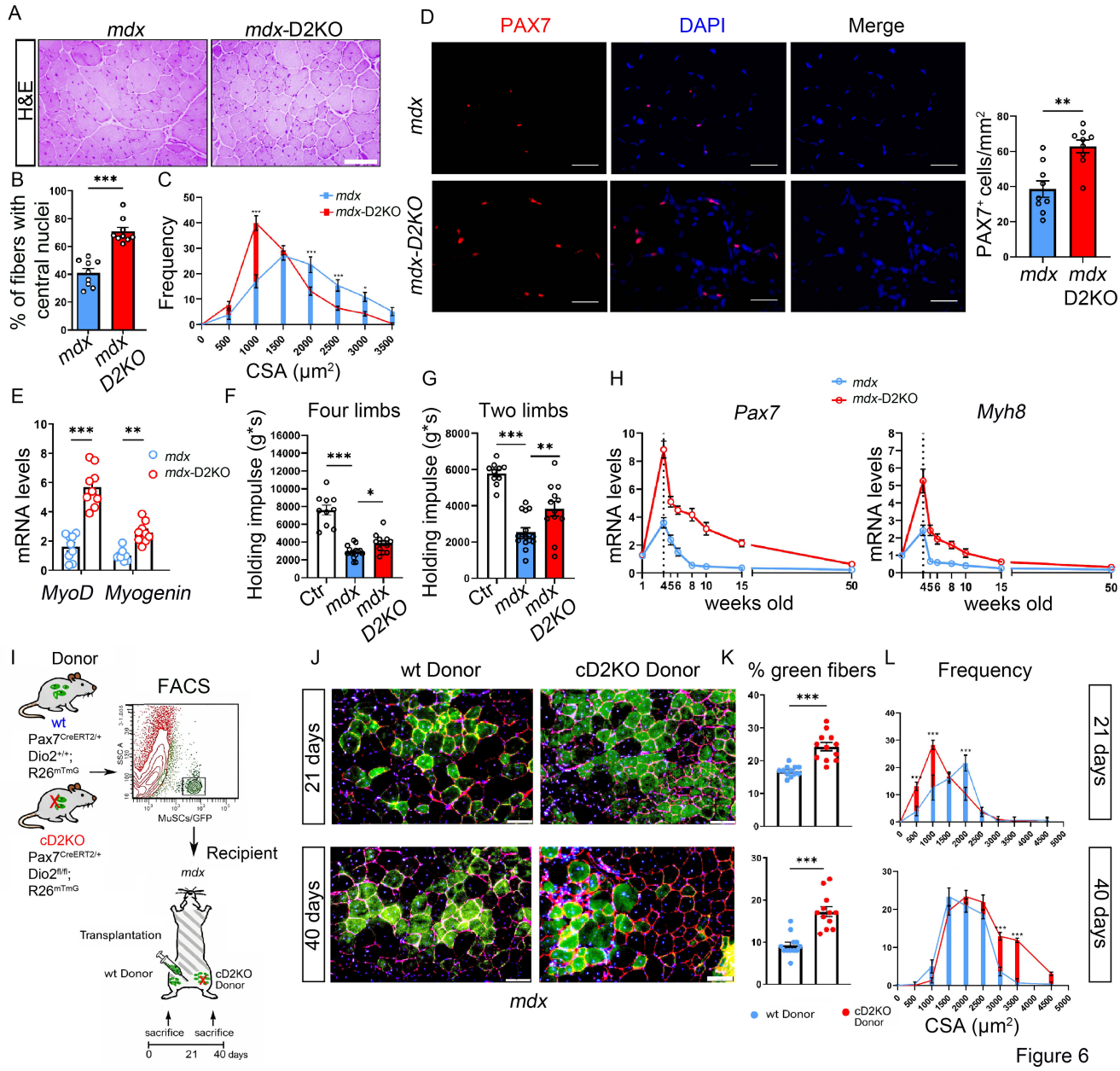

Figure 6

Figure 6. ***D2KO improves the phenotype of mdx mice.***

(A) Representative H&E of TA sections from mdx and mdx-D2KO mice (scale bar, 100 μm), n=9 for mdx and mdx-D2KO mice.

(B) Quantification of the percentage of fibers with central nuclei in mdx and mdx-D2KO mice.

(C) Quantification of the CSA.

(D) Representative IF staining of PAX7+ (scale bar, 100 μm) and their quantification (right).

(E) Relative mRNA levels of MyoD and Myogenin.

(F and G) Performance in four-limb (F) and two-limb (G) muscle strength hanging tests of controls (Ctr), mdx and mdx-D2KO mice at 4 weeks of age. n=10 ctr, n=15 mdx and n=12 mdx-D2KO mice.

(H) Pax7 and Myh8 mRNA levels from muscles at different weeks of age. Points represent the means ± SEM of at least three technical replicates (n=6 mdx and n=6 mdx-D2KO mice).

(I) Schematic representation of the D2-depleted MuSCs transplantation assay (I-L). MuSCs/GFP+ from wt ($Pax7^{creERT2/+}$; $D2^{+/+}$; $R26^{mTmG}$) and cD2KO ($Pax7^{creERT2/+}$; $D2^{fl/fl}$; $R26^{mTmG}$) mice were transplanted into the TA muscle of a single recipient mdx-mouse. n= 12 wt and n=12 cD2KO recipient mdx-mice.

(J) Representative IF staining of green epifluorescent fibers of mdx-mice xenografted as indicated. Laminin in red. Scale bar, 100 μm.

(K) Percentage of green epifluorescent fibers at 21 (upper) and 40 days (lower) following transplantation of MuSCs/GFP cells from wt and cD2KO donors.

(L) Quantification of the CSA (μm^2) of green fibers 21 (upper) and 40 days (lower) after xenografting. Bars represent the means ± SEM of at least three technical replicates.

Data are presented as mean ± SEM; *$p < 0.05$, **$p < 0.01$, ***$p < 0.001$ using a Mann-Whitney test when comparing two conditions, and 2-way ANOVA when comparing multiple conditions.. Each point (in B, D-G and K) represents the average of at least three technical replicates from each mouse.

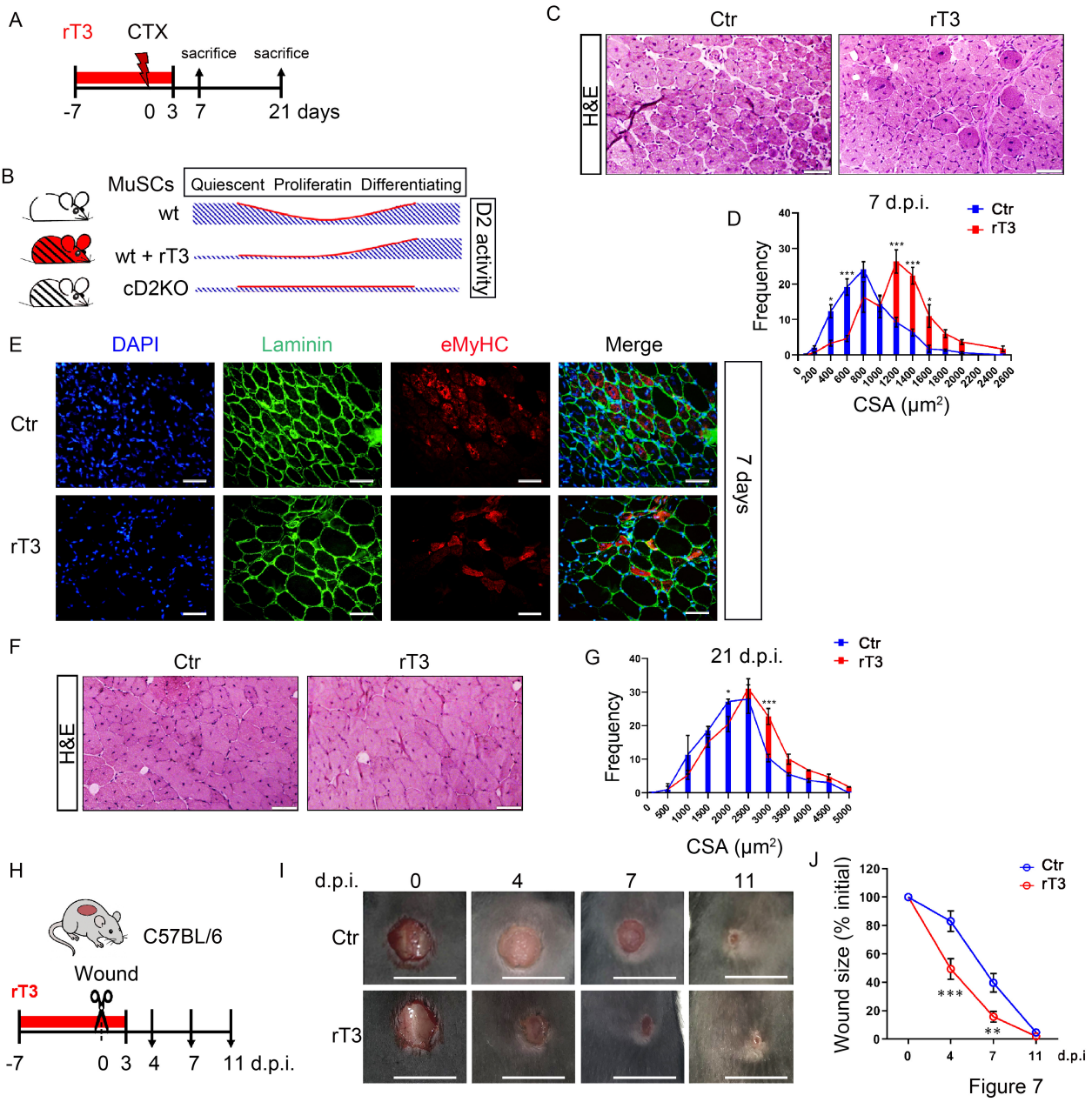

Figure 7. ***Pharmacological D2-blockade as an agent to enhance repair of muscle and skin injury.***
(A) Schematic diagram illustrating the experimental design (A-G). Two independent experiments were conducted (n=8 untreated and n=10 rT3-treated mice, each). In each experiment, n=4 untreated and n=5 rT3-treated mice were sacrificed at 7 and 21 days after CTX-injury, respectively.

(B) Schematic illustration of D2 activity in MuSCs during the myogenesis in untreated wild type, rT3-treated wild type and untreated cD2KO mice.
(C) Representative H&E staining of tibialis anterior sections (scale bar, 50 μm) from untreated (Ctr) and rT3-treated mice sacrificed 7 days after CTX injury.
(D) Quantification of the cross-sectional area of untreated (Ctr) and rT3-treated mice sacrificed 7 days after CTX-injury.
(E) Representative IF staining for eMyHC (red) and Laminin (green) in untreated (Ctr) and rT3-treated mice sacrificed 7 days after CTX injury.
(F) Representative H&E staining of tibialis anterior sections (scale bar, 50 μm) of untreated (Ctr) and rT3-treated mice sacrificed 21 days after CTX-injury.
(G) Quantification of the cross-sectional area of untreated (Ctr) and rT3-treated mice sacrificed 21 days after CTX-injury.
(H) Diagram of the experimental design of wound healing in untreated (Ctr) and rT3-treated mice (H-J). (n =12 wt mice and n=12 rT3 treated mice).
(I) Representative images of the wound healing experiment at wound creation (0) and after 4, 7, and 11 days.
(J) Quantification of wound closure as expressed in the mean percentage decrease compared to the initial wound size (scale bar, 1 cm). Data are presented as mean ± SEM; *$p < 0.05$, **$p < 0.01$, ***$p < 0.001$ using 2-way ANOVA.